How slab age and width combine to dictate the dynamics and evolution of subduction systems: a 3-D spherical study

Fangqin Chen[1], D. Rhodri Davies[1], Saskia Goes[2], Lior Suchoy[2], Stephan C. Kramer[2]

[1]Research School of Earth Sciences, The Australian National University, Canberra, ACT, Australia
[2]Department of Earth Science and Engineering, Imperial College London, London, UK

Key Points:

- Spherical models are used to examine the joint effect of slab age and width on free subduction dynamics.
- Older slabs enhance trench retreat whilst wider slabs can drive along-strike variations in shape.
- The effect of plate width is strongly modulated by plate age, given its control on trench retreat.

Corresponding author: Fangqin Chen, Fangqin.Chen@anu.edu.au

Abstract

Many of the factors expected to control the dynamics and evolution of Earth's subduction zones are under-explored in an Earth-like spherical geometry. Here, we simulate multi-material free-subduction of a complex rheology slab in a 3-D spherical shell domain, to investigate the effect of plate age (simulated by covarying plate thickness and density) and width on the evolution of subduction systems. We find that the first-order predictions of our spherical cases are generally consistent with existing Cartesian studies: (i) as subducting plate age increases, slabs retreat more and subduct at a shallower dip angle, due to increased bending resistance and sinking rates; and (ii) wider slabs can develop along-strike variations in trench curvature due to toroidal flow at slab edges, trending towards a 'W'-shaped trench with increasing slab width. We find, however, that these along-strike variations are restricted to older, stronger, retreating slabs:. Younger slabs that drive minimal trench motion remain relatively straight along the length of the subduction zone. We summarise our results into a regime diagram, which highlights how slab age modulates the effect of slab width, and present examples of the evolutionary history of subduction zones that are consistent with our model predictions.

Plain Language Summary

Subduction zones are locations where Earth's tectonic plates collide, and the denser plate subsequently descends into the mantle. They exert important controls on surface plate motions, plate boundary deformation, mountain-building, seismic hazard, volcanism, and help to organise underlying mantle flow, which is the engine driving our dynamic Earth. As a result, this important process has been extensively studied through both analogue and computational models. Here, we model the dynamics and evolution of subduction systems on an Earth-like sphere, and find that: (i) older plates, which have spent longer cooling at Earth's surface, sink into the underlying mantle faster, at a shallower angle; and (ii) narrower plates tend to develop 'C'-shaped trenches, whereas wider plates tend to develop 'W'-shaped trenches. Importantly, the influence of subducting plate width is strongly dependent on its age. We show how these two factors combined can explain key aspects of the evolution of several major subduction zones on Earth.

1 Introduction

During subduction, the oceanic lithosphere of one tectonic plate dives beneath another at a convergent margin and is recycled into Earth's mantle (e.g., Stern, 2002; Kearey et al., 2009). As subducted slabs descend, their negative buoyancy provides a key driving force for plate tectonics, and they continue to influence surface processes in a number of ways (e.g., Forsyth & Uyeda, 1975; Mitrovica et al., 1989; Lithgow-Bertelloni & Richards, 1998; Wheeler & White, 2002; Perrin et al., 2018; Rubey et al., 2017; Beall et al., 2021). Seismic images of Earth's interior reveal that when slabs descend towards the mantle transition zone, at depths of 410–660 km that coincide with several mineralogical phase transformations and a likely viscosity increase (e.g., Hager & Richards, 1989), some stall and are horizontally deflected (e.g., the Ryuku, Izu-Bonin and Honshu slabs), some thicken and buckle (e.g., the Marianas slab), whilst others appear to pass through unhindered (e.g., the Cocos and Antilles slabs). Their imaged morphologies are therefore far from uniform (e.g., Karato et al., 2001; Li et al., 2008; Fukao & Obayashi, 2013a; Goes et al., 2017; van der Meer et al., 2018). The dominant controls on such variations remain unclear, and likely vary between different subduction zones, due to complexities arising from non-linear and multi-scale interactions between several aspects of the mantle system, including downgoing and overriding plate properties, global mantle flow, mineral phase changes and material rheology (e.g., Karato et al., 2001; Čížková et al., 2002; Capitanio et al., 2007; Schellart et al., 2007; Goes et al., 2008; Stegman, Farrington, et

al., 2010; Garel et al., 2014; Goes et al., 2017; Agrusta et al., 2017; Alsaif et al., 2020; Holt & Royden, 2020; Garel et al., 2020; Suchoy et al., 2021).

The observational record does not support a clear correlation between slab morphology and subducting plate age (e.g., Lallemand et al., 2005; Sdrolias & Müller, 2006; Goes et al., 2011). This implies that other factors strongly influence the evolution of subduction systems, including variations in a slab's age along the trench, trench width, local sources of buoyancy such as oceanic plateaus and aseismic ridges, regional tectonics, and complexities associated with overriding plates. Several studies have investigated how these aspects control the evolution of subducted slabs, mostly in either 2-D or 3-D Cartesian domains, in an attempt to reconcile predictions from geodynamical modelling with the observed morphologies (e.g., Morra et al., 2006; Čížková et al., 2007; Schellart et al., 2007; Capitanio et al., 2010; Martinod et al., 2010; Mason et al., 2010; Stegman, Farrington, et al., 2010; Rodríguez-González et al., 2012; Sharples et al., 2014; Garel et al., 2014; Čížková & Bina, 2015; Holt et al., 2018).

The age of a subducting slab determines its thermal structure, which controls slab thickness, density and rheology. In turn, these control slab buoyancy and strength, which combine to determine the rate of trench retreat (e.g., Bellahsen et al., 2005; Capitanio et al., 2007; Di Giuseppe et al., 2008; Schellart, 2008; Ribe, 2010; Stegman, Farrington, et al., 2010; Garel et al., 2014; Goes et al., 2017). It is well-established that trench-motion history correlates with slab morphology (e.g., van der Hilst & Seno, 1993; Faccenna et al., 2001; Goes et al., 2017). Goes et al. (2008) suggest that older, colder, oceanic lithosphere is stronger due to the temperature dependence of viscosity, and that this drives significant trench retreat, with slabs more likely to lie flat at the mantle transition zone; conversely, younger lithosphere is weaker and subducts with less trench retreat, tending to buckle at the mantle transition zone. This direct link between slab age and the style of slab-transition zone interaction is supported by laboratory and numerical simulations (e.g., Schellart, 2004; Bellahsen et al., 2005; Capitanio et al., 2007; Funiciello et al., 2008; Garel et al., 2014; Goes et al., 2017).

Slab width also plays an important role in determining the evolution of subduction zones, affecting the shape and curvature of the trench, by influencing the rate of trench retreat (e.g., Bellahsen et al., 2005; Stegman et al., 2006; Schellart et al., 2007; Stegman, Schellart, & Freeman, 2010; Strak & Schellart, 2016). Schellart et al. (2007) advocate an inversely proportional relationship between trench migration rates and the width of subduction zones. In their models, wider slabs develop upper mantle stagnation zones, where the centre of the trench exhibits negligible trench retreat relative to its edges. Such a relationship is observed in large subduction systems such as the South American subduction zone, and could be responsible for the varying styles of slab morphology observed along wide trenches.

Plate interactions and lateral variations in plate properties also influence the geometry and evolution of subducting slabs. The structure and motion of overriding plates have an effect on slab dip, trench migration, and slab interaction with the mantle transition zone (e.g., Jarrard, 1986; Lallemand et al., 2005; Heuret et al., 2007; Capitanio et al., 2010; van Dinther et al., 2010; Garel et al., 2014). Interactions with nearby past or ongoing subduction zones may also affect the sinking velocity and slab penetration of the mantle transition zone (e.g., Fukao et al., 2009; Becker & Faccenna, 2011; Fukao & Obayashi, 2013b; Čížková & Bina, 2019). The subduction of locally thickened oceanic lithosphere, such as oceanic plateaus, aseismic ridges or seamount chains, has been proposed to influence the shape of the trench and change the geometry of subducting slabs (e.g., Cross & Pilger, 1982; Gutscher, Malavieille, et al., 1999; Martinod et al., 2005; Capitanio et al., 2011; Suchoy et al., 2022). The higher compositional buoyancy of oceanic plateaus and ridges could resist slab sinking into the mantle and, thus, potentially lead to flat slab subduction (e.g., van Hunen et al., 2002; Mason et al., 2010). These factors

add to the complexity of observed slab morphology, and may explain why no simple correlations can be made with plate properties.

Existing numerical and laboratory studies in an enclosed Cartesian domain provide valuable insight into the sensitivity of slab morphology to a number of these controlling parameters. However, such models neglect the role of Earth's sphericity, the geometric consequences of which results in curved subduction zones, the build-up of lateral strain, buckling along the trench, and an increase in the geometric stiffness of slabs (e.g., Frank, 1968; Laravie, 1975; Bayly, 1982; Fukao et al., 1987; Yamaoka, 1988; Tanimoto, 1998; Mahadevan et al., 2010; Schettino & Tassi, 2012).

In this paper, our aim is to investigate the effect of subducting plate age and width on slab morphology using 3-D spherical shell numerical models of free subduction. Only a limited number of spherical subduction models have investigated the dynamics of subduction, and these considered only isoviscous plates (e.g. Morra et al., 2009, 2012; Butterworth et al., 2012, 2014; Chamolly & Ribe, 2021). To more realistically approximate subduction on Earth, especially for wider plates, we will present the first multi-material subduction models with a composite plate rheology in a spherical shell domain. We consider plate ages (estimated with three combinations of plate thickness and density) ranging from young (~ 10 Myr, estimated using a half space cooling model) to old (~ 140 Myr),

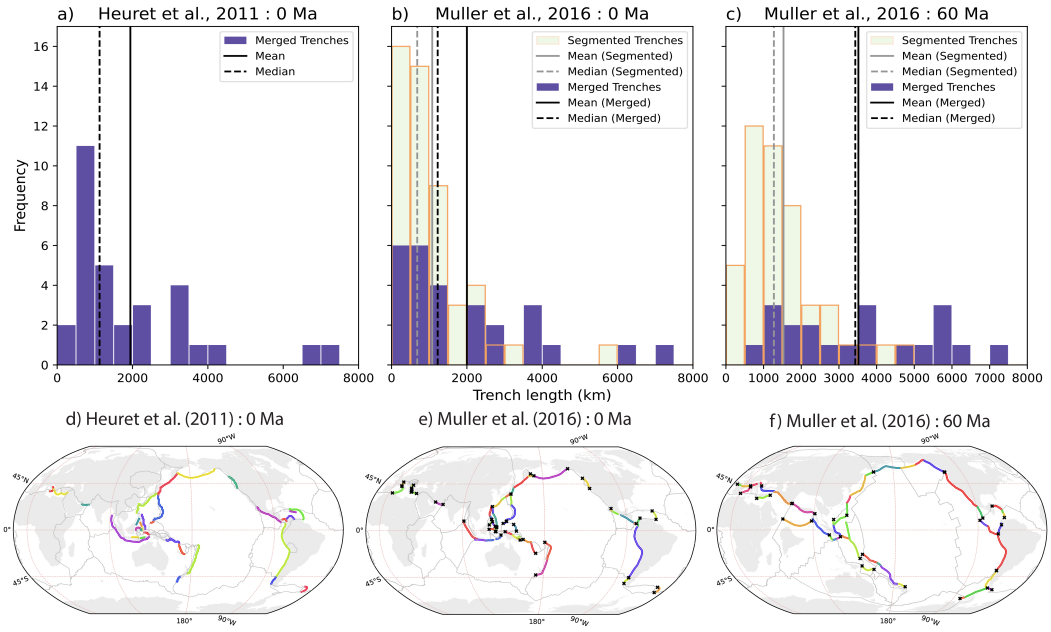

Figure 1. (a) Present-day trench length histogram compiled from rupture segment lengths by Heuret et al. (2011) and combined here for commonly recognised continuous trenches; (b) and (c) trench length histograms based on global tectonic plate reconstructions, at the present day and at 60 Ma, respectively Müller et al. (2016). The reconstructed trenches are segmented based on changes in lower or upper plate characteristics (green bars with orange outline). Based on lower plate properties, we merged segments that likely subduct as coherent slabs (purple bars). (d) Map of subduction zones from Heuret et al. (2011). (e) and (f) Map of trench segments based on plate reconstruction at present and at 60 Ma by Müller et al. (2016). In (e) and (f), black crosses represent edges of subduction zones. Trench segments within each subduction zone were merged when calculating trench length.

noting that the range of subducting plate ages on Earth at present day is 0 - 160 Myr (e.g. Müller et al., 2016). Motivated by a compilation of global trench lengths at the present day (Heuret et al., 2011) and Cenozoic Era reconstructions (Müller et al., 2016), we examine trench widths of 1200, 2400, 3600 and 4800 km. As illustrated in Figure 1, at the present day, most trenches are less than 5000 km wide, with mean and median widths of 1940 km and 1130 km for the dataset of Heuret et al. (2011) and 2000 km and 1230 km for the dataset of Müller et al. (2016). At 60 Ma (where there are less data on narrow trenches), mean and median widths are 3520 km and 3430 km (Müller et al., 2016). It is noteworthy that very few trenches exceed 6000 km in width: at present, the South America trench is 7060 km wide, and the Andaman-Sumatra-Java-Timor trench exceeds 6040 km width; at 60 Myr, the South America and Aleutian trenches were $\sim$ 7100 and $\sim$ 6070 km wide, respectively (Müller et al., 2016).

In this paper, we present, for a systematic set of simulations, a quantitative comparison to demonstrate how slab thickness and density (approximating the buoyancy of slabs of different age) and slab width affects the evolution of subducting slabs. We then discuss the likely mechanisms that can explain our results and their implications for an improved understanding of subduction on Earth.

2 Model Description

2.1 Governing Equations and Numerical Strategy

We simulate multi-material free-subduction of a composite visco-plastic plate into an ambient mantle, in a 3-D hemispherical shell domain, which extends from the surface to the core-mantle-boundary (CMB) at a depth of 2890 km. Assuming incompressibility, the governing equations for this problem are the continuity equation,

$$\nabla \cdot u = 0 \tag{1}$$

the conservation of momentum equation for infinite Prandtl number,

$$-\vec{\nabla} p + \nabla \cdot \left[\mu \left(\vec{\nabla} u + \left(\vec{\nabla} u \right)^T \right) \right] = g \Delta \rho \Gamma \hat{k} \tag{2}$$

and an advection equation for composition,

$$\frac{\partial \Gamma}{\partial t} + \mathbf{u} \cdot \vec{\nabla} \Gamma = 0 \tag{3}$$

where u is velocity, p the pressure, μ the viscosity, ρ the density, g gravity acceleration, $\hat{k}$ unit vector in the direction opposite gravity, and Γ the material volume fraction ($\Gamma = 1$ in a region occupied by a given material and $\Gamma = 0$ elsewhere).

Simulations are carried out using Fluidity (e.g., Davies et al., 2011; Kramer et al., 2012; Davies et al., 2016), an anisotropic, adaptive, unstructured mesh computational modelling framework supporting finite element and control volume discretisations. Fluidity has recently been validated for simulations in a spherical shell domain against an extensive set of analytical solutions introduced by Kramer et al. (2021). It has also been validated for visco-plastic simulations like those examined herein (e.g. Le Voci et al., 2014; Tosi et al., 2015). In the context of this study, Fluidity has several favourable features. The framework: (i) uses an unstructured mesh, which enables the straightforward representation of complex geometries and materials; (ii) dynamically optimizes this mesh, across parallel processors, providing increased resolution in areas of dynamic importance, thus allowing for accurate simulations across a range of length-scales, within a single model; (iii) enhances mesh optimization using anisotropic elements; (iv) can employ a free-surface boundary condition, which is important for correctly capturing slab decoupling from the surface (Kramer et al., 2012); (v) utilises the highly-scalable parallel linear system solvers available in PETSc (Balay et al., 1997, 2021a, 2021b), which can efficiently handle sharp,

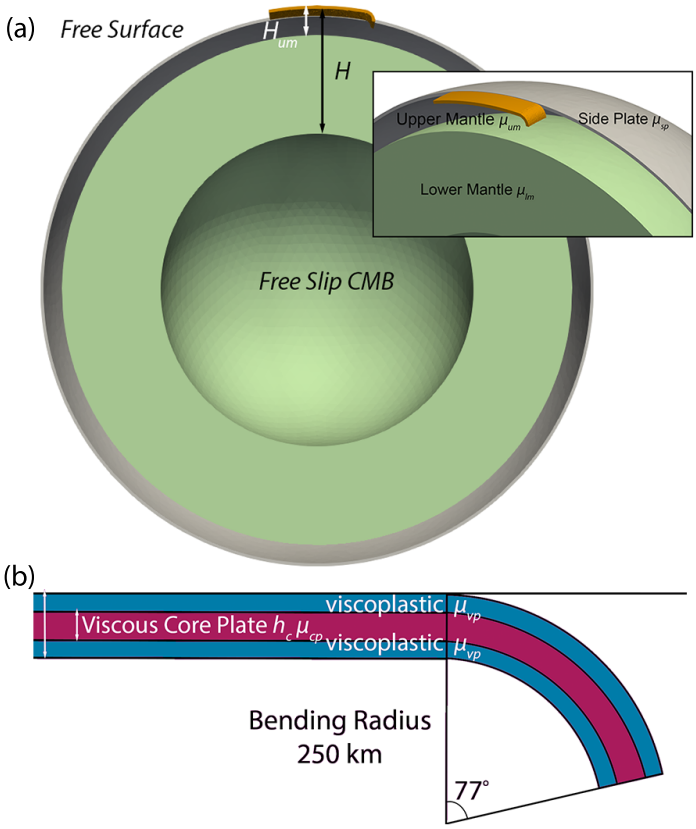

Figure 2. (a) Setup of our simulations in a spherical geometry. We exploit the symmetry of the system, allowing us to halve the computational domain's extent, whilst inner and outer boundaries approximate Earth's core-mantle-boundary and surface, respectively. (b) Initial slab tip geometry of our layered visco-plastic plates.

orders of magnitude variations in viscosity; and (vi) has a novel interface-preservation scheme, which conserves material volume fractions and allows for the incorporation of distinct materials (Wilson, 2009). In this study, Fluidity's adaptive mesh capabilities are utilised to provide a local resolution of 3 km in regions of dynamic significance (i.e. at the interface between materials and in regions of strong velocity and viscosity contrasts), with a coarser resolution of up to 300 km elsewhere. It is this adaptive mesh functionality that makes our spherical shell simulations computationally tractable.

2.2 Geometry, Boundary Conditions and Material Properties

The configuration of our models is inspired by Stegman, Farrington, et al. (2010) and Garel et al. (2014). Simulations exploit the symmetry of the system to halve the computational domain's extent, modelling half of the plate width in a hemispherical shell. When non-dimensionalised, the hemispherical shell has an outer radius of 2.22 and an inner radius 1.22, thus the computational domain has a thickness of 1. Models have a free-surface boundary condition on the outer surface, and a free-slip condition on the symmetry plane and CMB, as illustrated in Figure 2 (a). Gravity acts radially, towards the centre of the sphere.

Table 1. Parameters common to all simulations.

Parameter	Symbol	Value
Gravitational acceleration	g	10 m/s^2
Characteristic depth (whole mantle)	H	2890 km
Depth of upper mantle	H_{um}	660 km
Upper mantle reference viscosity	μ_{um}	2.0×10^{20} Pa s
Lower mantle reference viscosity	μ_{lm}	$50 \times \mu_{um}$
Core plate viscosity	μ_{cp}	$100 \times \mu_{um}$
Initial viscosity of visco-plastic layer	μ_{Newt}	$100 \times \mu_{um}$
Side plate viscosity	μ_{sp}	$1000 \times \mu_{um}$
Mantle density	ρ	3300 kg/m^3
Yield stress	τ_{yield}	100 MPa

The subducting plate length (L) is 2200 km. The initial slab tip geometry is prescribed with a bending radius of 250 km and an angle of 77°, resulting in a 336 km-long slab tip (Figure 2b). The subducting lithosphere comprises a composite plate of constant initial thickness with a core isoviscous layer embedded in upper and lower visco-plastic layers with viscosities that follow a von Mises law. Upper and lower visco-plastic layers are used to approximate the strain-rate weakening that occurs above and below the slab core in thermo-mechanical simulations of subduction (e.g. Garel et al., 2014), following OzBench et al. (2008). Upper and lower layers are assigned the minimum viscosity between the Newtonian viscosity μ_{Newt} and an effective von Mises viscosity μ_{vM}, such that purely viscous deformation occurs as long as the second invariant of the stress tensor $\tau_{II} = 2\mu\dot{\varepsilon}_{II}$ (where $\dot{\varepsilon}_{II}$ is the second invariant of strain rate tensor) does not reach the critical yield stress, τ_{yield}. The effective viscosity of the visco-plastic layers is given by:

$$\mu_{\text{vM}} = \begin{cases} \frac{\tau_{II}}{2\dot{\varepsilon}_{II}}, & \text{if } \tau < \tau_{\text{yield}} \\ \frac{\tau_{\text{yield}}}{2\dot{\varepsilon}_{II}}, & \text{if } \tau \geq \tau_{\text{yield}} \end{cases} \tag{4}$$

At material interfaces, the average viscosity is calculated through a geometric mean,

$$\mu_{\text{ave}} = \mu_1^{\Gamma_1} \mu_2^{\Gamma_2}, \tag{5}$$

where μ_i is the viscosity of material i, and Γ_i is the relative volume fraction of material i in the vicinity of the finite-element node at which the effective viscosity μ_{ave} is needed.

The subducting plate is surrounded by mantle material, with no overriding or trailing plate. When the plate advances, the mantle material fills in behind the trailing edge. A dome-shaped side plate covers the entire domain adjacent to the subducting plate. It has the same thickness as the subducting plate, and is placed 22 km away from the plate's edge, keeping a constant distance from the symmetry plane around the base of the dome. The side plate is 1000 times more viscous than adjacent upper mantle material, and prevents lateral flow from narrowing the width of downgoing plate (as in Holt et al., 2017). The lower mantle below 660 km depth is 50 times more viscous than the upper mantle. The viscosity jump is a simplified parameterisation of the transition zone's hindering effect of the mantle flow from upper mantle into lower mantle, from not only the viscosity increase with depth but also the endothermic phase transition that is excluded from the model, as in Stegman, Farrington, et al. (2010). Model parameters common to all simulations are listed in Table 1.

Table 2. Simulations examined and associated model parameters.

Case	h (km)	h_c (km)	$\Delta\rho$ (kg m^{-3})	w (km)
W1200_young	45	15	40	1200
W1200_ref	70	30	80	1200
W1200_old	100	40	120	1200
W2400_young	45	15	40	2400
W2400_ref	70	30	80	2400
W2400_old	100	40	120	2400
W3600_young	45	15	40	3600
W3600_ref	70	30	80	3600
W3600_old	100	40	120	3600
W4800_young	45	15	40	4800
W4800_ref	70	30	80	4800
W4800_old	100	40	120	4800

2.3 Cases Examined and Quantitative Model Diagnostics

We investigate 12 cases across a wide parameter-space. We systematically varied plate width (w) and plate 'age', represented by co-varying plate thickness (h), core thickness (h_c), and density contrast between the plate and adjacent mantle ($\Delta\rho$) to capture the joint increase of negative plate buoyancy and bending strength with age. This allows us to examine how these two factors influence the evolution of subduction and slab morphologies. Our choices are motivated by subduction regime diagrams, as a function of plate age or plate width, from other studies (e.g., Stegman, Schellart, & Freeman, 2010; Garel et al., 2014; Goes et al., 2017). The selected combinations of plate thickness and density contrast produce diverse subduction behaviours, ranging from a vertical-folding type young plate to a retreating and flattening old plate. We note that in the following sections, specified plate widths refer to the full width of the plate (i.e. twice the width simulated, owing to the symmetry plane). Case names, alongside their key parameter values, are listed in Table 2.

To quantify the sensitivity of results to these parameters, we have calculated several diagnostic outputs. When doing so, the boundary of the slab is defined as the 0.5 contour of the mantle material volume fraction (material volume fraction = 1 when the material is mantle, 0 otherwise). Based on this contour, we extract the slab tip depth, the trench location (measured at 15 km depth), and the trailing edge position, as well as rates of slab descent, trench retreat and plate advance. We extract the fastest vertical sinking velocity at the symmetry plane; as well as the maximum sinking velocity throughout the entire domain. We calculate the average slab dip in the upper mantle from the surface to 650 km depth, with respect to the direction of gravity at the slab centre at 325 km depth, which is radially towards the centre of the sphere from the point of measurement. Measurements are taken at the symmetry plane unless otherwise specified. We also trace the evolution of trench geometry relative to the initial trench shape.

3 Results

3.1 Reference Case

Case W1200_ref is selected as our reference, given its mid-range plate buoyancy and thickness (McKenzie et al., 2005), and width that sits towards the lower end of trench lengths on Earth. The temporal evolution of this case is illustrated in Figure 3(a). As subduction starts, the slab tip steepens. During the upper mantle sinking phase (Fig-

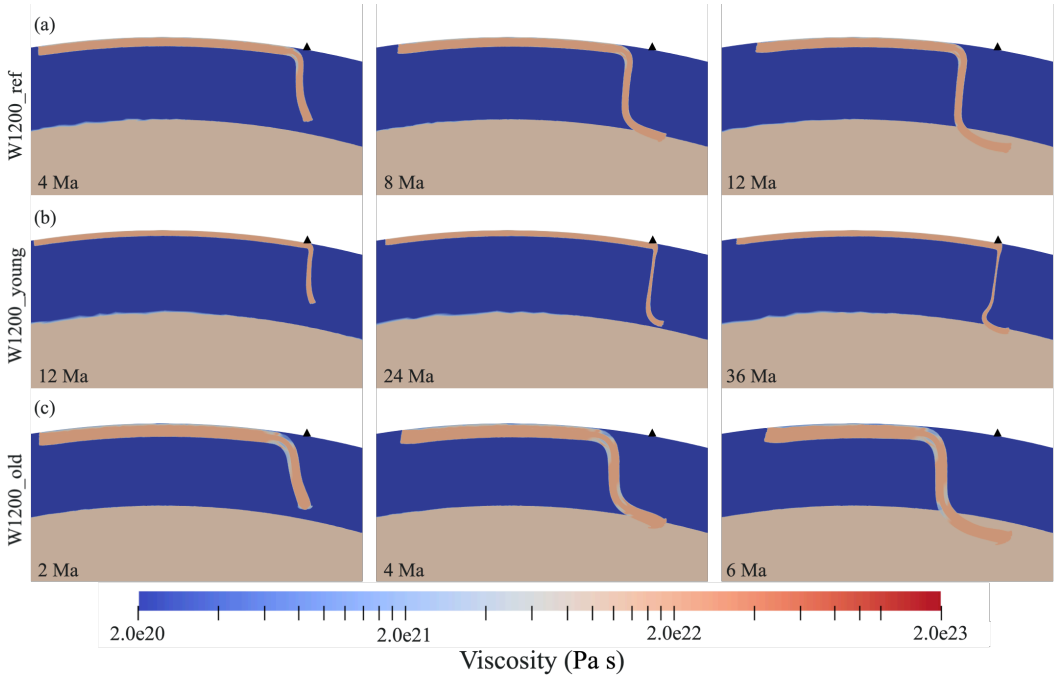

Figure 3. Snapshots illustrating the spatio-temporal evolution of slab morphology as reflected in the viscosity field, for models with a plate width of 1200 km: (a) W1200_ref, with $H = 70\,\mathrm{km}$ and $\Delta\rho = 80\,\mathrm{kg\,m^{-3}}$; (b) W1200_young, with $H = 45\,\mathrm{km}$ and $\Delta\rho = 40\,\mathrm{kg\,m^{-3}}$; (c)W1200_old, with $H = 100\,\mathrm{km}$ and $\Delta\rho = 120\,\mathrm{kg\,m^{-3}}$.

ure 4a), the trench steadily retreats from its initial position (Figure 4b) with ∼50% of subduction accommodated via this trench retreat (over 60% in the early stages), despite the trailing edge of the plate advancing steadily (Figure 4c,d). As the trench retreats, it develops a concave 'C' shape, as illustrated in Figure 5(b). Following interaction with the viscosity jump at 660 km depth, the slab tip is deflected, the slab sinking rate reduces substantially (Figure 4a,e), and the upper mantle section of the slab steepens (Figure 4f). The slab then slowly sinks into the lower mantle.

Coupling between the sinking plate and the adjacent mantle drives toroidal and poloidal mantle flow (e.g., Schellart, 2004; Funiciello et al., 2006; Stegman et al., 2006). Figure 6(a-c) illustrates horizontal flow at 300 km depth at different stages of subduction: trench/slab retreat drives toroidal flow around the edge of the plate, which promotes increased trench concavity (Figure 5b). Figure 6(d-f) shows vertical cross-sections through the symmetry plane: two poloidal cells can be identified as the slab sinks in the upper mantle, one above the downgoing plate in the mantle wedge, and the other in the sub-slab region. During the upper-mantle phase of subduction, the mantle wedge cell is more prominent, while flow velocities in this cell diminish as the slab tip deflects and sinks into the more viscous lower mantle.

3.2 Influence of subducting plate age

The two cases, W1200_young and W1200_old, were designed to demonstrate how plate age (through its joint effect on buoyancy and strength) modifies subduction dynamics. Our parameter values approximate the properties of younger (decreased $\Delta\rho$ and H) and older (increased $\Delta\rho$ and H) plates, respectively.

The younger slab (W1200_young) stretches and sinks almost vertically through the upper mantle as it subducts, folding upon interaction with the upper-lower mantle interface (Figures 3b and 4e). Trench location remains almost fixed (Figure 4b) and trench shape does not evolve much over time (Figure 5a). Excluding the initial phase of subduction, trench retreat is minimal: within 5 Myr of the start of subduction, $\sim 80\%$ of subduction is accommodated by plate advance (Figure 4d).

The older case (W1200_old) exhibits the fastest sinking, trench retreat and plate advance velocities among all cases examined at this width (Figure 4). The slab tip sinks in the upper mantle at a shallower angle than the younger cases (Figure 4f). It is deflected at the mantle transition zone, and the sinking rate decreases as the slab moves into the lower mantle (Figure 4a,e). Similar to the reference case, after reaching 660 km depth, the upper mantle portion of the slab gradually steepens (Figure 3c). Trench retreat is substantial and accommodates much of the subduction (the trench retreat to total descent ratio remains above $\sim 55\%$ throughout the simulation – Figure 4b,d), with the trench developing a concave curvature over time (Figure 5c).

The cases examined at 1200 km width clearly display a range of behaviours, with a strong sensitivity to the age, i.e. buoyancy and strength, of the subducting slab. The younger plate exhibits the weakest behaviour, manifested by a steeper upper mantle subduction angle and minimal trench retreat, with subduction principally accommodated via plate advance. This case falls into the vertical folding regime (e.g., Schellart, 2008; Stegman, Farrington, et al., 2010; Garel et al., 2014; Goes et al., 2017). The older plate

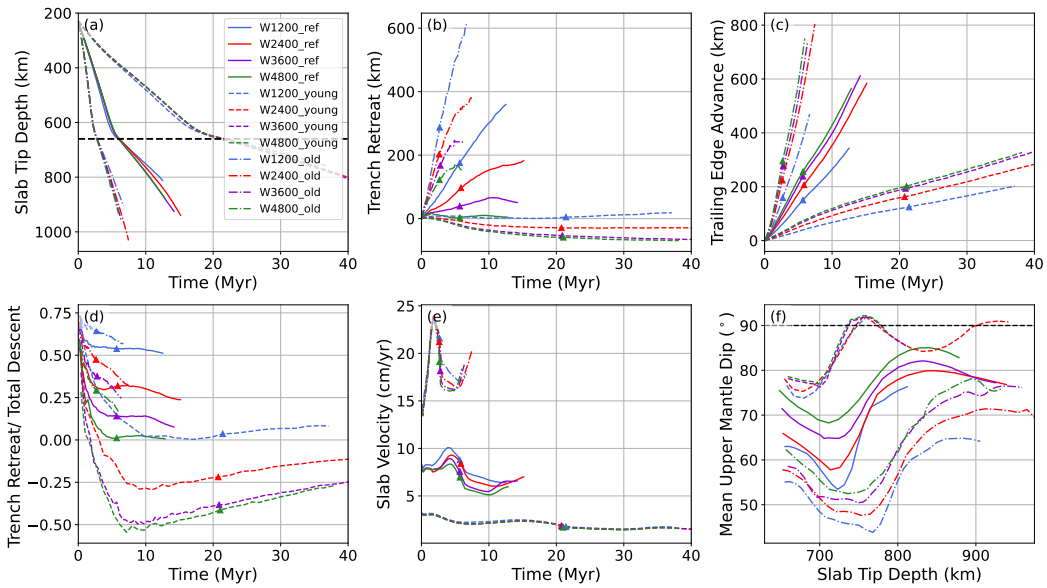

Figure 4. Comparison between all simulations: (a) slab tip depth, as a function of time, where the upper–lower mantle boundary is indicated by the black dotted line at 660 km depth; (b) amount of trench retreat; (c) amount of plate advance, measured at the plate's trailing edge; (d) ratio of trench retreat to total length of plate subducted, which is the sum of trench retreat and trailing edge advance; (e) slab sinking velocity; and (f) average slab dip in the upper mantle, with the black dashed line indicating a vertical slab with dip angle of 90°. Triangles indicate the time where the slab tip starts interacting with the base of the upper mantle at 660 km depth. All measurements are taken at the symmetry plane.

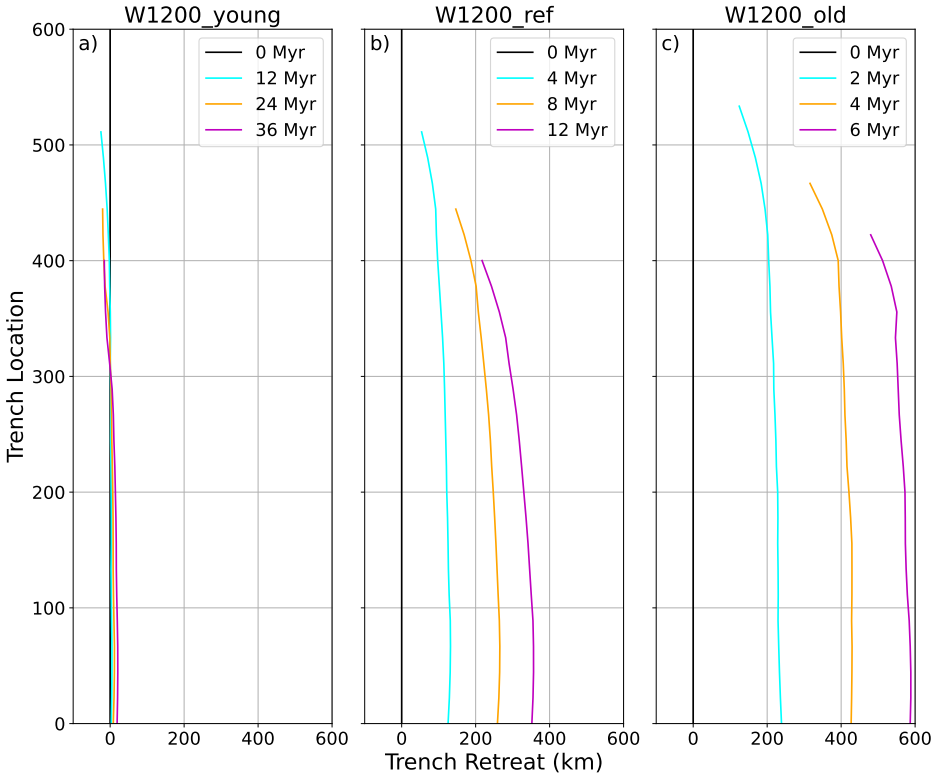

Figure 5. Spatio-temporal evolution of trench location of cases with a plate width of 1200 km. Times given in Myr since simulation initiation. (a) young: $H = 45\,\mathrm{km}$, $\Delta\rho = 40\,\mathrm{kg\,m^{-3}}$; (b) reference: $H = 70\,\mathrm{km}$, $\Delta\rho = 80\,\mathrm{kg\,m^{-3}}$; (c) old: $H = 100\,\mathrm{km}$, $\Delta\rho = 120\,\mathrm{kg\,m^{-3}}$.

is the strongest: it sinks faster, has a shallower upper mantle subduction angle, and drives significant trench retreat, with more than half of the subduction accommodated via this retreat (Figure 4). This case falls into the weak retreat regime (e.g., Schellart, 2008; Stegman, Farrington, et al., 2010; Garel et al., 2014; Goes et al., 2017). As expected, the reference case has an intermediate strength, with sinking and trench-retreat rates, in addition to the slab dip angle, all between those of the older and younger cases (Figure 4). As trench retreat accounts for slightly more than $\sim 50\%$ of the total subduction in the reference case, it also falls into the weak retreat regime.

3.3 Effect of subducting plate width

We next examine cases with the same buoyancy and strength combinations as in the previous section, but at larger widths of 2400 km, 3600 km and 4800 km.

3.3.1 Trench retreat

For cases that share a common plate age, a larger plate width reduces trench retreat. As the slab tries to maintain its sinking rate, this results in stronger bending at the trench. The dynamical behaviour can lead to a shift in subduction regime, especially at the centre of the plate, where increased slab width causes slabs to steepen at the trench, with the trench sometimes advancing. The behaviour at the centre of the plate thereby shifts towards a 'bending mode', where slab bending at the trench takes up a significant part of the potential energy of the slab, as opposed to a 'sinking mode', where bending

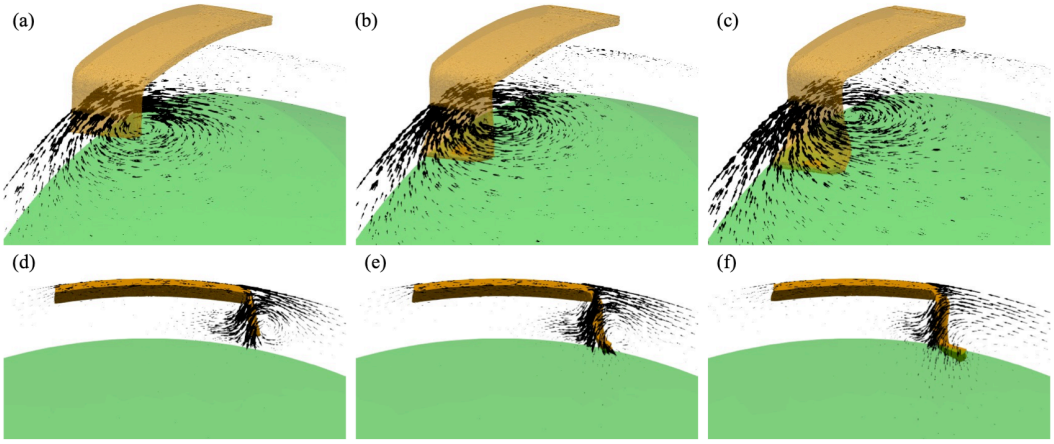

Figure 6. Snapshots of upper mantle flow regime for a plate width of 1200 km, of reference age (plate thickness of 70 km and $\Delta\rho$ of 80 kg m^{-3}). (a)-(c) Flow tangential to the radial direction at 300 km depth, highlighting the toroidal flow cell at the edge of the plate. The largest arrows represent a tangential velocity magnitude of 3.7 cm/yr (radial component of velocity removed); (b)-(d) Corresponding poloidal flow cells, in the mantle wedge and sub-slab regions. The largest arrow in the bottom panels represents a velocity magnitude of 9.4 cm/yr. As the slab tip interacts with the mantle transition zone, the poloidal cell diminishes as the viscosity increase in the lower mantle hampers return flow beneath the slab tip.

at the trench uses only 10-20% of the potential energy, and slab sinking is, in part, achieved through trench retreat (e.g. Capitanio et al., 2007; Ribe, 2010).

For younger cases, at all widths (W2400_young, W3600_young and W4800_young), slabs stretch and sink steeply in the upper mantle, at a dip of $> 75°$ (Figures 4f), eventually buckling upon interaction with the transition zone at 660 km depth, like their narrower counterpart (Figure 7). However, as plate width increases, the rate of trench advance also increases. Upon interaction with the upper-lower mantle boundary, the 1200 km-wide cases display minimal trench motion, whereas the trench has advanced $\sim$ 30 km, $\sim$ 50 km and $\sim$ 50 km for the 2400 km, 3600 km and 4800 km wide cases, respectively (Figure 4b). This folding, with some advance, is a characteristic of a 'fold-and-retreat' bending mode (e.g., Schellart, 2008; Stegman, Farrington, et al., 2010; Goes et al., 2017), and the centre of wide young slabs display behaviour between a vertical folding and fold-and-retreat mode.

For wider cases at the reference age (W2400_ref, W3600_ref and W4800_ref), slabs retreat prior to interacting with the base of the upper mantle. At the symmetry plane, they steepen and buckle following interaction, thus exhibiting stronger bending at the trench in comparison to the 1200 km-wide case, which displayed a deflect-and-sink behaviour (Figure 3a). As plate width increases, the upper mantle portion of the slab steepens (Figures 4f, 7). Buckled slabs with a width of 4800 km have maximum dips that exceed those of the 2400 km wide case by $\sim 4°$. At the symmetry plane, the trench retreat:total subduction ratio decreases with plate width ($\sim$ 0.5, $\sim$ 0.25, $\sim$ 0.1, and $\sim$ 0 for 1200 km, 2400 km, 3600 km and 4800 km wide cases respectively – Figure 4d), indicating less of a role for trench retreat in accommodating subduction. This is most clearly demonstrated for the W4800_ref simulation, which transitions from retreat at a width of 1200 km, to stagnation at a width of 4800 km (Figures 4d).

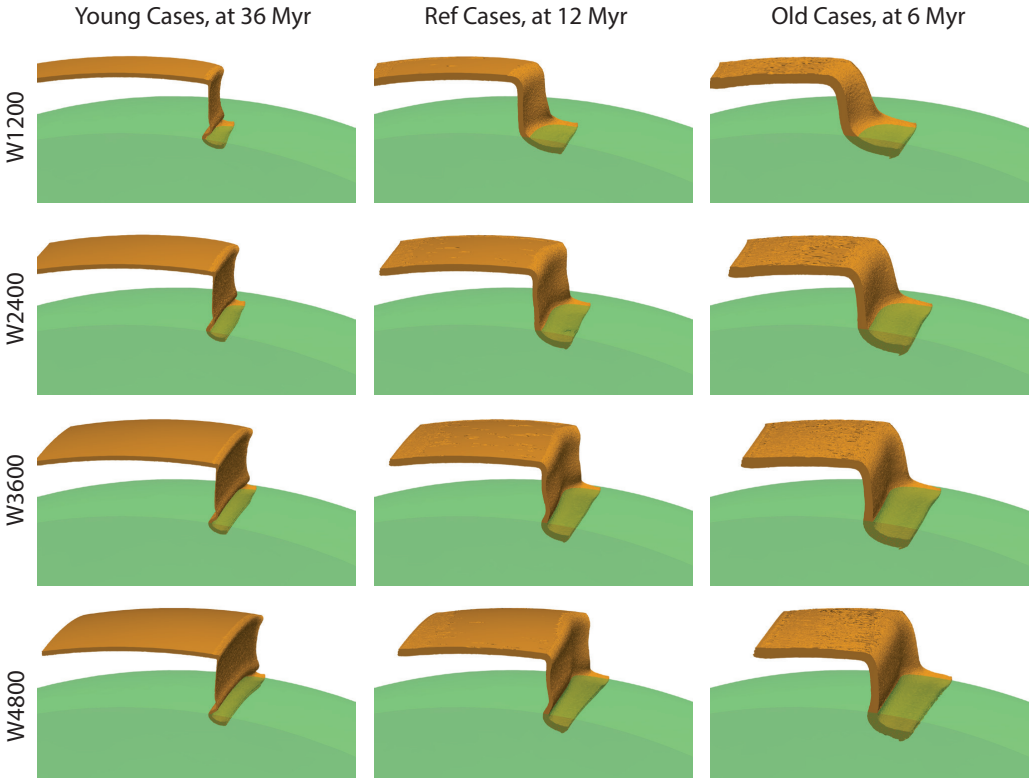

Figure 7. Final stage of model slab morphology. From top to bottom, models with plate widths of 1200 km, 2400 km, 3600 km, and 4800 km are shown, respectively. From left to right, we show the young cases at 36 Myr, reference cases at 12 Myr, and old cases at 6 Myr, respectively.

For older cases at widths of 2400 km (W2400_old), 3600 km (W3600_old), and 4800 km (W4800_old), slabs sink with shallower angles than corresponding reference age cases in the upper mantle (Figures 4f, 7), deflecting at transition zone depths and, subsequently, sinking through into the lower mantle. As plate width increases from 1200 km to 4800 km, the maximum upper mantle dip angle increases by $\sim 14°$. The trench retreat:total subduction ratio also decreases as slab width increases, from ~ 0.6 to ~ 0.3 to ~ 0.25 to < 0.2 for 1200 km, 2400 km, 3600 km and 4800 km wide slabs, respectively. While the older cases across all widths fall into the weak retreat regime, the wider cases (W3600_old and W4800_old) exhibit a significant reduction in trench retreat post interaction with the transition zone (Figures 4b).

Taken together, our results demonstrate that as plate width increases, slabs display less of a tendency to retreat across all three ages examined. As a consequence, they bend more strongly at the trench.

3.3.2 Trench curvatures and along strike variations in morphology

Different trench shapes are observed across the simulations examined, which can be categorised into 3 types: (i) 'I'-type, where the trench is reasonably straight (e.g., Figure 5a); (ii) 'C'-type, where trench retreat is strongest in the centre of the slab relative to its edges (e.g., Figure 5b); and (iii) 'W'-type, where trench retreat is low in the cen-

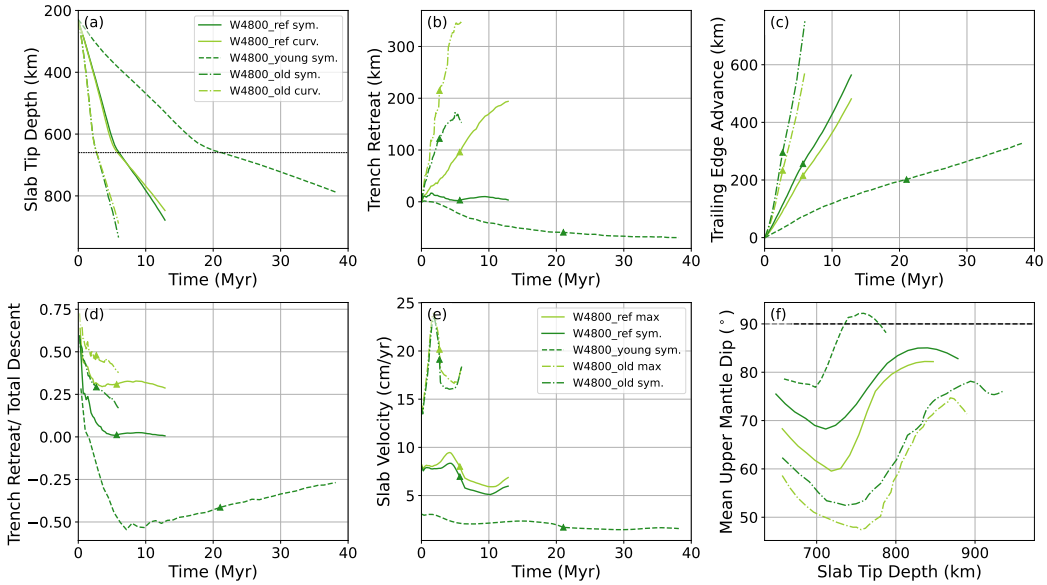

Figure 8. Comparison between simulations with a plate width of 4800 km. Measurements are taken at the centre of the slab (i.e., the symmetry plane, abbreviated to sym.) and the location of most trench retreat, which is at the centre of the concave curvature (curv.). (a) slab tip depth, as a function of time, where the upper–lower mantle boundary is indicated by the black dotted line at 660 km depth; (b) amount of trench retreat; (c) amount of plate advance, measured at the plate's trailing edge; (d) ratio of trench retreat to total length of plate subducted, which is the sum of trench retreat and trailing edge advance; (e) slab sinking velocity at the symmetry plane, and the maximum down-going radial velocity (abbreviated to max); and (f) average slab dip in the upper mantle, with the black dashed line indicating a vertical slab with dip angle of 90°. Triangles indicate the time of slab tip interaction with the upper-lower mantle interface.

tre of the slab and at the edges, and higher in between ('S' curvature in half-width, as shown in Figure 11b).

We find that 'I'-type trenches develop for younger cases across all plate widths: trenches remain reasonably straight, aside from a slight curvature adjacent to the slab edge (Figures 5a, 9a, 10a and 11a). 'C'-type trenches develop for narrow plates that are retreating, for example, in cases W1200_ref and W1200_old (Figure 5b,c). For stronger plates that have moderate width, such as case W2400_old (Figure 9b), the trench develops a gentle curvature close to the edge, but the bulk of the trench remains approximately straight throughout the simulation, in an elongated 'C' shape. As slab width increases, 'W'-type trenches develop in slabs that would have 'C'-type trenches at a narrower width. This can be seen by comparing cases W2400_ref, W3600_ref and W4800_ref. Case W2400_ref develops a concave curvature at the edges, with the centre of the trench retreating slightly less than the edge (Figure 9b), placing it at the transition between 'C'- and 'W'-type trenches. Conversely, case W3600_ref and case W4800_ref display a 'W'-type curvature (Figure 10b and Figure 11b). Similarly, for older slabs, wider trenches develop into a 'W' shape ('S' in half-width in Figure 11c). In case W4800_old, the curvature increases following slab transition-zone interaction and the difference in trench retreat between the centre and the region of most retreat also increases (Figure 8b).

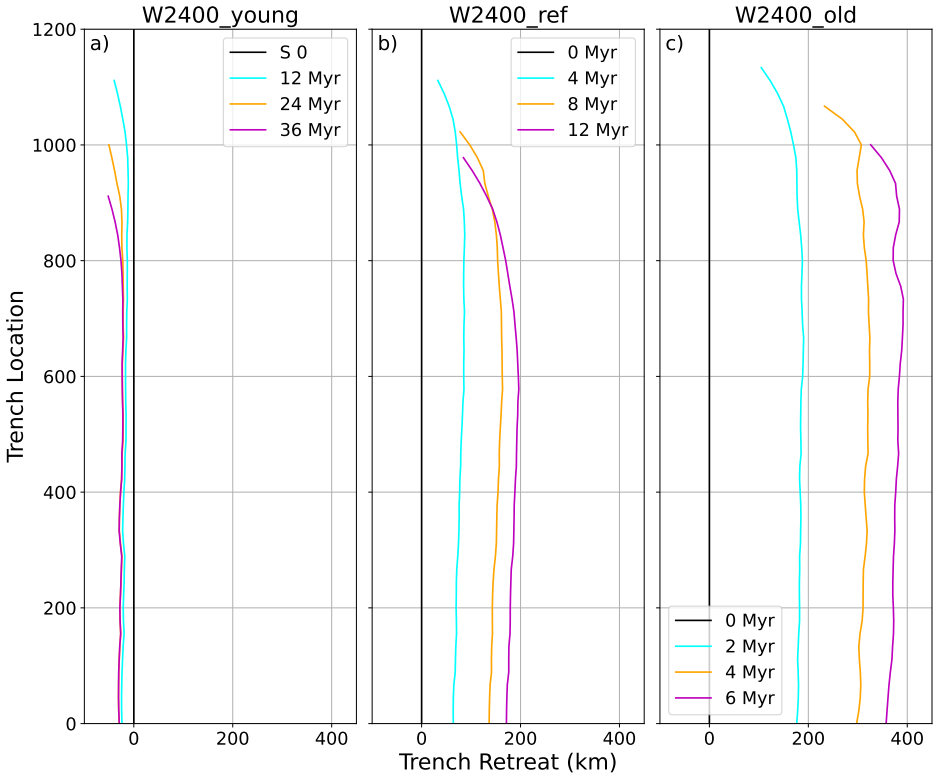

Figure 9. Spatio-temporal evolution of trench location in simulations with a plate width of 2400 km. Times given in Myr since simulation initiation. (a) young: $H = 45\,\mathrm{km}$, $\Delta\rho = 40\,\mathrm{kg\,m^{-3}}$; (b) reference: $H = 70\,\mathrm{km}$, $\Delta\rho = 80\,\mathrm{kg\,m^{-3}}$; (c) old: $H = 100\,\mathrm{km}$, $\Delta\rho = 120\,\mathrm{kg\,m^{-3}}$.

Taken together, our results demonstrate that the evolution of trench shape is dependent on both slab age and slab width. Younger and weaker slabs that are in the vertical folding regime develop mostly straight 'I'-type trenches, regardless of slab width. For older cases that can drive trench retreat, trench curvatures evolve from a 'C'-shape in narrower plates to a 'W'-shape in wider plates, with slabs of greater strength transitioning to a 'W' shape at a greater width.

Slab morphologies evolve with trench shape. For weaker cases with an 'I'-type trench, subducting slab morphology is relatively uniform along strike (Figure 12a). For stronger wide retreating cases that develop a 'W'-type trench, along-strike variations in trench retreat translate into morphological variations at depth (Figures 12b,c and 8a): at the symmetry plane, the slab is steep and buckles at the transition zone, with dips up to 9° larger than in the slab at the location of most retreat, where the slab deflects at transition-zone depths (Figure 8d,f).

4 Discussion

4.1 Role of Subducting Plate Age and Width

Our results demonstrate that the evolution of subduction systems is strongly sensitive to slab age (due to its effect on buoyancy and strength), which is consistent with several previous studies (e.g., Capitanio et al., 2007; Schellart, 2008; Stegman, Farrington, et al., 2010; Garel et al., 2014). Slabs with greater negative buoyancy and slab pull

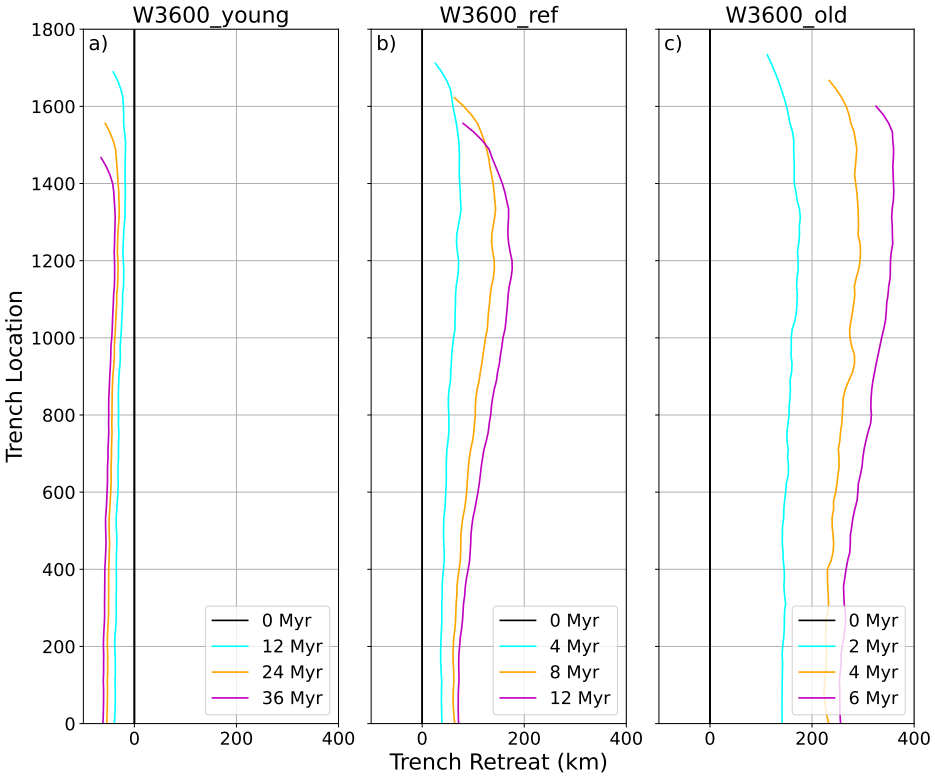

Figure 10. Spatio-temporal evolution of trench location in simulations with a plate width of 3600 km. Times given in Myr since simulation initiation. (a) young: $H = 45\,\mathrm{km}$, $\Delta\rho = 40\,\mathrm{kg\,m^{-3}}$; (b) reference: $H = 70\,\mathrm{km}$, $\Delta\rho = 80\,\mathrm{kg\,m^{-3}}$; (c) old: $H = 100\,\mathrm{km}$, $\Delta\rho = 120\,\mathrm{kg\,m^{-3}}$.

promote increased upper mantle sinking velocities (e.g., Stegman, Farrington, et al., 2010; Garel et al., 2014; Goes et al., 2017). Slab thickness determines slab strength (alongside buoyancy), with thicker slabs possessing a higher bending resistance (e.g., Conrad & Hager, 1999; Bellahsen et al., 2005; Ribe, 2010; Capitanio & Morra, 2012) and, accordingly, taking longer to bend at the trench. The regime that a subduction system falls into depends on a delicate balance between the amount of time taken to bend (larger for thicker slabs) and the sinking time (larger for younger slabs) (Ribe, 2010). Taken together, in younger slabs (low slab pull – longer sinking times; low slab strength – shorter bending times), bending dominates over trench retreat, with slabs typically subducting steeply and buckling upon interaction with the upper-lower mantle boundary, owing to the high angle of incidence. Conversely, in older slabs (high slab pull – shorter sinking times; high slab strength – longer bending times), there is insufficient time for substantial bending at the trench, with subduction accommodated principally through trench retreat. As a a result, slabs typically exhibit a shallower upper mantle dip angle, which facilitates slab deflection and stagnation at the base of the upper mantle (e.g., Torii & Yoshioka, 2007; Čížková & Bina, 2013; Garel et al., 2014; Agrusta et al., 2017).

The evolution of 'C'- and 'W'-shaped trenches for our retreating cases are similar to results from Schellart et al. (2007), with curvature at slab edges induced by toroidal flow around and into the slab. Interplay between the size and strength of the toroidal cell, the width of the slab, and the slab's resistance to along-strike bending, dictate how trench shape responds. The size of the toroidal cell determines over what region along the trench the plate experiences significant force from the adjacent mantle flow and, hence,

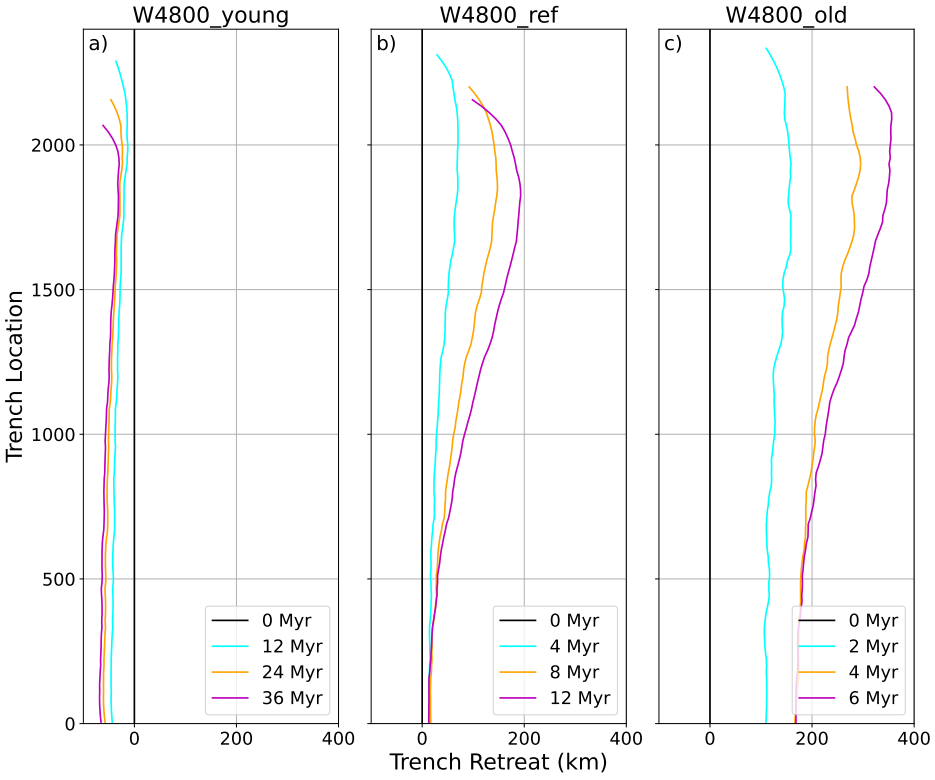

Figure 11. Spatio-temporal evolution of trench location in simulations with a plate width of 4800 km. Times given in Myr since simulation initiation. (a) young: $H = 45\,\mathrm{km}$, $\Delta\rho = 40\,\mathrm{kg\,m^{-3}}$; (b) reference: $H = 70\,\mathrm{km}$, $\Delta\rho = 80\,\mathrm{kg\,m^{-3}}$; (c) old: $H = 100\,\mathrm{km}$, $\Delta\rho = 120\,\mathrm{kg\,m^{-3}}$.

the location of potential concave curvature development. The strength of the toroidal cell is determined by the amount of trench retreat. The width of the plate relative to the size of the toroidal cell determines the distance between the toroidal cells at both edges. When these factors are coupled with the plate's resistance to bending, the evolution of trench shape can be understood. 'C'-shaped trenches are observed for narrow plates, where toroidal cell sizes are close to half of the slab width (Figure 6). 'W'-shaped trenches are observed for wider plates, where the size of the toroidal cell is substantially smaller than the width of the plate: the centre of such plates are thus not markedly influenced by toroidal flow (Figure 13a). Plates with less resistance to bending along strike can develop enhanced curvature at the trench (W3600_ref, Figure 10b); conversely, plates with a higher strength can prevent significant curvature development at the trench, remaining in a relatively uniform elongated 'C'-shape rather than evolving into a 'W'-shape (e.g., W3600_old, Figure 10c).

While the influence of plate width on subduction dynamics has been studied previously (e.g., Stegman et al., 2006; Schellart et al., 2007; Di Giuseppe et al., 2008), our results demonstrate that the important role of width is strongly modulated by the age of the plate and its effect on plate strength. The change from a 'C'-shaped trench to a 'W'-shaped trench with increasing width only occurs for cases that are initially in a retreating regime (i.e., older plates). For younger plates that are in the vertical folding regime, increasing plate width has little impact on along-strike variability, because these plates do not subduct through trench retreat and, hence, cannot generate toroidal cells of the

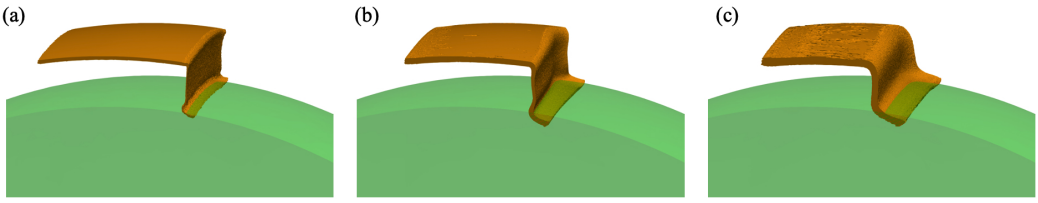

Figure 12. 3-D morphology of cases with different ages at a width of 4800 km: (a) young: $H = 45\,\mathrm{km}$, $\Delta\rho = 40\,\mathrm{kg\,m^{-3}}$; (b) reference: $H = 70\,\mathrm{km}$, $\Delta\rho = 80\,\mathrm{kg\,m^{-3}}$; (c) old: $H = 100\,\mathrm{km}$, $\Delta\rho = 120\,\mathrm{kg\,m^{-3}}$. Young cases have relatively uniform morphology along-strike, whereas older cases (b,c) display varying morphologies: vertically folding at the centre, but horizontally deflecting closer to the edge.

intensity required to induce trench deformation (Figure 13b). Accordingly, the younger cases develop 'I'-type trench shapes across all widths examined in this study.

Variations in the amount of trench retreat also translate into along-strike morphological variations at depth. These variations can also be understood by the along-strike influence of toroidal flow, facilitating trench retreat. Vertical folding morphologies correspond to (parts of the) slabs with limited trench retreat or minor advance, while retreating segments lead to shallower dips and deflection at the base of the upper mantle. While all wide slabs display the typical morphology of the vertical folding regime at the centre, the young models have tight buckles, whereas older slabs have open folds with larger bending radii. This difference in bending radii illustrates that older slabs have higher bending resistance and strength than younger slabs, despite falling into the same subduction regime. Overall, as plate width increases, the center of the slab shifts from sinking to bending, due to the lack of toroidal flow and its role in driving trench retreat.

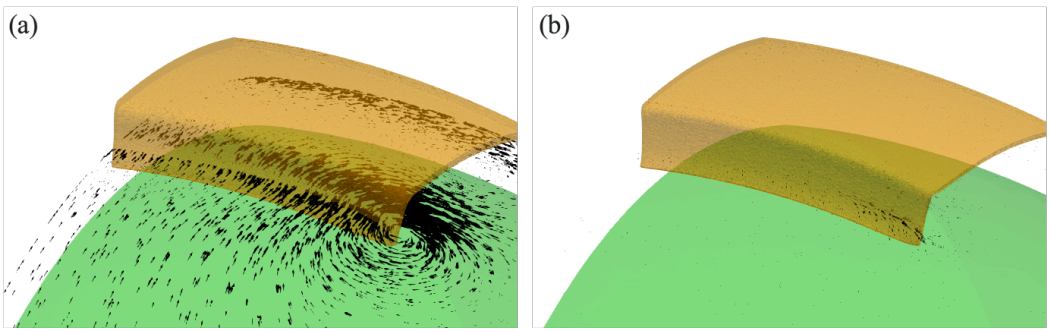

Figure 13. Lateral flow patterns at 300 km depth for: (a) case W4800_ref; and (b) case W4800_young. The length and direction of the arrows illustrates the magnitude and direction of tangential velocities (i.e. after the radial component has been removed). In both panels, the largest arrow represents a tangential velocity magnitude of 2.5 cm/yr. For the reference age case in (a), a toroidal cell can be identified at the edge of the slab, which does not extend to the centre of the slab. For the younger case in (b), although there is some toroidal flow around the edge of the slab, its magnitude and area of influence is insignificant when compared to the reference case.

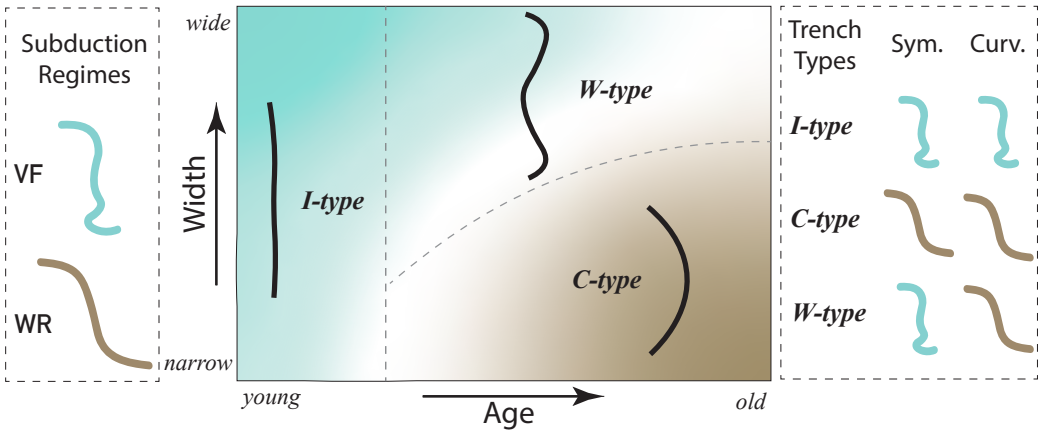

Figure 14. Schematic diagrams of how age and width, affect subduction styles and trench shape. Regimes: VF - vertical folding; WR - weak retreat. The three trench types 'I', 'C' and 'W' are separated into three approximate domains, by gray dashed lines, with slabs that lie on domain boundaries at the transition between two trench types. Slab behaviours that are in VF at the symmetry plane are represented by the cyan region, and those in WR are represented by the brown region. The rightmost panel illustrates the slab morphology at the centre of the slab (i.e., the symmetry plane, abbreviated to sym.) and the location of most trench retreat, which is at the centre of the concave curvature (curv.). For young plates, the subduction regime is VF regardless of the width of the plate, and trench shapes are mostly straight, indicated by 'I'-type. As age increases, it is easier to drive trench retreat and slabs fall into the WR regime; but as width increases, the centre of the plate shifts towards the VF regime. Beyond a certain age, the narrower and/or older plates tend to develop 'C'-type trenches; wider and/or younger plates tend to develop 'W'-type trenches.

The competing roles of plate age and plate width in dictating the subduction style are summarised via a regime diagram in Figure 14.

4.2 Implications for Subduction on Earth

Our model predictions across different plate ages and widths, can be used to analyse how these aspects combine to control the spatio-temporal evolution of trenches on Earth. While Earth's subduction zones are substantially more complex than those considered in our simulations, due to a multitude of factors including subducting plates of non-uniform age, the subduction of buoyant anomalies, and the influence of overriding plates, the 'I', 'C' and 'W' trench shapes predicted by our models are consistent with present-day trench shapes (e.g. Bird, 2003; Schellart et al., 2007; Heuret et al., 2011) and those in reconstructions of plate motion histories through the Cenozoic Era (Müller et al., 2016, 2019).

4.2.1 'I'-type Trenches

Our results demonstrate that 'I'-shape trenches typically develop when a young plate subducts with negligible trench motion, regardless of trench width. The tectonic reconstructions of Müller et al. (2019) provide some examples of young plate subduction during the Cenozoic, such as the subduction of the Izanagi plate at the Japan trench at 50–

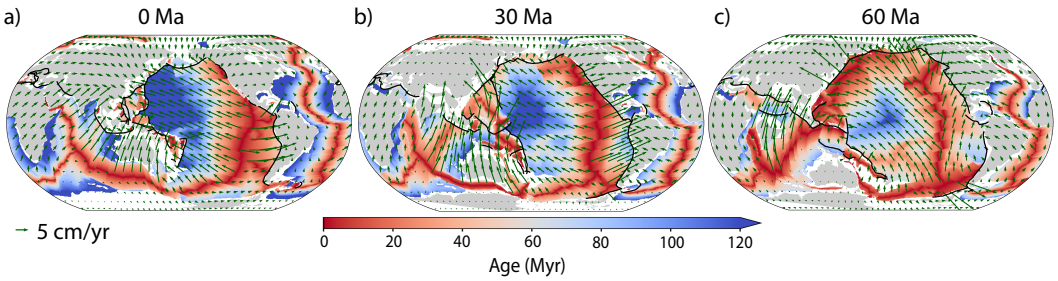

Figure 15. Maps of ocean-floor age and trench positions (black lines) based on the plate reconstruction by Müller et al. (2019) at: (a) the present-day; (b) 30 Ma; and (c) 60 Ma. Green arrows represent plate velocity (in the mantle reference frame of the reconstruction). For reference, present day coastlines are shown in light grey.

60 Ma and the subduction of the Farallon plate below North America prior to ∼ 30 Ma (Figure 15).

As illustrated in Figure 16, the Japan subduction zone was relatively straight (apart from its northern end) with minimal trench motion between 50 and 60 Ma, characteristics typical of 'I'-type trenches. The trench measured ∼ 5000 km in width, and a young plate (∼ 10 Myr) was subducted along the whole trench (Figure 15c). As time advanced past 50 Ma, the main part of the trench evolved from an 'I'-type towards a 'C'-type example, with increasing trench retreat, trench curvature and trench segmentation (Figure 16a). This is coincident with an increase in subducting plate age, as shown in Figure 15(a,b), after the subduction of the Izanagi-Pacific ridge at ∼ 50 Ma (Kimura et al., 2019).

Similarly, the reconstructed North America trench displayed an 'I'-type shape prior to 30 Ma, when the very young (∼ 10 Myr at 30 Ma) Farallon plate was subducting beneath North America, as shown in Figure 15(b). Prior to 30 Ma, the trench shape was relatively straight, with very little trench retreat, particularly from 30−50 Ma (Figure

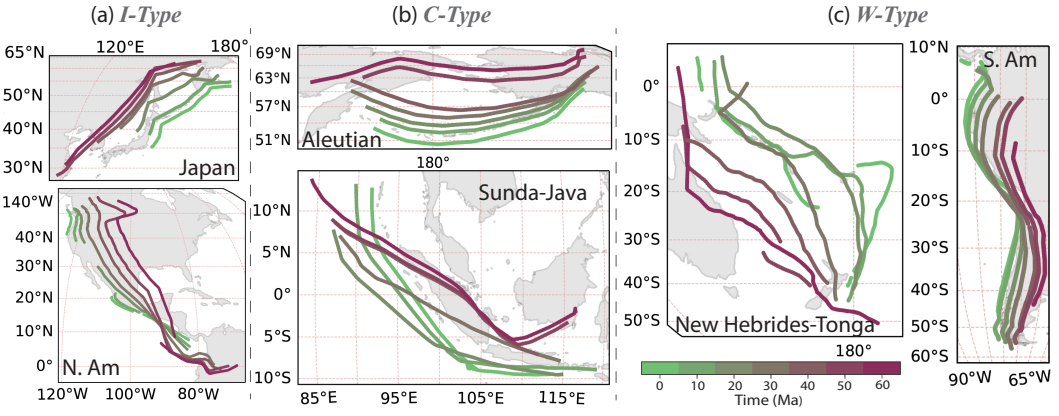

Figure 16. Examples of 'I' shape (a), 'C' shape (b) and 'W' shape (c) trenches based on the plate reconstruction by Müller et al. (2019), where trenches are drawn at 10 Myr intervals. N.Am - North America; S.Am - South America.

16). Following breakup of the Farallon Plate in the mid-Cenozoic, into the Juan de Fuca, Cocos and Nazca Plates (e.g., Atwater, 1970; Lonsdale, 2005), the continuity of the 5900 km-wide trench was lost, and the strike-slip San Andreas Fault developed on the west coast of North America.

4.2.2 'C'-type Trenches

Our results suggest that 'C'-shape trenches should be associated with moderate to old subducting plate ages and moderate slab widths. 'C'-shape trenches are the most common trench shape observed on Earth. The Aleutian subduction zone and the Sunda-Java subduction zone are two examples of 'C'-shape trenches that developed during the Cenozoic (Figure 16). Although both trenches have also been affected by buoyant structures on the incoming plate (such as the Yakutat terrane below Alaska and Australian continental crust impinging on the Banda part of the Sunda-Java arc), we propose that the combined width and age of the downgoing plate exerted an important control on the evolution of trench shape.

The Aleutian trench extends ~ 4000 km from the south coast of Alaska to Kamchatka (Scholl et al., 1975). Prior to 40 Ma, the Kula plate subducted at the eastern side of the Aleutian trench, and the Pacific plate subducted at the western side. Subduction of young oceanic lithosphere ($\sim 10-40$ Myr at 60 Ma) along the trench (Figure 15c) resulted in a gentle curvature, with a shape between 'C'- and 'I'-types (Figure 16, Müller et al., 2019). At 40 Ma, when the Pacific plate had started subducting at the Aleutian trench; the age of the subducting plate increased and the Aleutian trench retreated and developed a 'C'-shape curvature, with enhanced curvature in the west (Figure 16). This is consistent with our modelling predictions, and could be related to the non-uniform subducting plate age at the Aleutian trench: the subducting Pacific plate is younger to the east (currently ~ 10 Myr) and older to the west (~ 120 Myr at present, Figure 15a,b), with the older part of the plate driving more retreat, generating the asymmetric 'C'-shaped trench.

The Sunda-Java trench also has a complex subduction history. Prior to 43 Ma, the active Wharton ridge was subducting beneath Sumatra, but since then the ridge has become inactive (Whittaker et al., 2007). As a result, the majority of material subducted prior to 43 Ma was young (~ 10 Myr old – Figure 15c), leading to minimal trench motion at the Sunda-Java subduction zone, consistent with 'I'-type subduction (Figure 16b). As the Wharton ridge ceased spreading and the subducting plate age increased (Figure 15a,b), the trench began to retreat and developed a 'C' shape across its ~ 5000 km width, again demonstrating that an 'I'-type to 'C'-type transition can occur when subducting plate age increases, consistent with our modelling predictions.

4.2.3 'W'-type Trenches

'W'-type trenches develop with moderate and older subducting plate age and very wide trenches. The South American trench is the textbook example of a 'W'-shape (Schellart et al., 2007): it exhibits concave curvature on both edges, with the centre of the trench almost stagnant throughout the Cenozoic (Figure 15c). Subduction in the South Pacific also exhibits 'W'-type characteristics in the early Cenozoic.

The South American trench is over 6000 km long, and subducted moderately old material ($\sim 50-80$ Myr) throughout the Cenozoic at the centre of the trench (Figure 15). Trench evolution shows increasing oroclinal bending through the Cenozoic (Schepers et al., 2017) and, hence, more retreat towards the north and south than in the central part at the Bolivian bend (Figure 16, Müller et al., 2019). The present-day trench shape is typical of our wide plate model predictions, where the Bolivian Orocline is located close to the centre of the trench, while sections of the trench close the edges have a concave

geometry. The subduction of pre-existing buoyant features on the Nazca Plate and interaction with varying thickness upper plate are further complexities that likely added to its evolution towards the current geometry (e.g., Gutscher, Olivet, et al., 1999; Espurt et al., 2008; Capitanio et al., 2011). However, although it is likely that multiple factors contribute to the shape of the trench at the South America Subduction Zone, our results agree with the previous suggestion by Schellart et al. (2007) that the first-order 'W'-shape is dictated by its large width, modulated by its moderate subducting-plate age.

The South Pacific region has a relatively complex tectonic history. In the early Cenozoic, old Pacific plate was subducting under the South Pacific trench, which had length exceeding 6000 km (Figure 15c). The trench at 60 Ma has characteristics of a 'W'-shape. There is a region of low trench retreat near 20° S, where the oldest ($\sim$ 100 Myr) part of the plate was subducting. The trench is concave north and south of this point. As the trench evolves, the northern and southern ends of it start to evolve separately, and the shorter trench takes on a 'C' type shape (Figure 16, 15c). Post 20 Ma, in response to arrival of the buoyant Ontong-Java plateau (Neal et al., 1997; Mann & Taira, 2004; Stotz et al., 2017) the trench segments further into the New Hebrides, New Britain and Tonga-Kermadec-Hikurangi trenches (e.g., Pelletier et al., 1998). These different stages of evolution and the shape of the resulting trenches were likely preconditioned by the original 'W' shape.

Overall, the examples of 'I'-, 'C'- and 'W'-shape trenches on Earth are in line with our modeling results. 'I'-type trenches are associated with very young downgoing plates of $\sim$ 10 Myr old; and as plate age increases, some transition into 'C'-shape trenches. 'W'-shape trenches are observed in subduction zones exceeding 6000 km width, where older material (greater than 50 Myr old) is being subducted, thus driving trench retreat. There is no doubt that the trench shape at each subduction zone is further modulated by additional complexities, including variable downgoing plate age along strike, subduction of buoyant active or bathymetric ridges, variations in thickness and buoyancy of the upper plate, and large tectonic reconfiguration events such as the India-Eurasian collision. Nonetheless, our results demonstrate the key role that both subducting plate age and width play in controlling the evolution of trench geometry, providing a framework to better understand the evolution of subduction zones.

5 Conclusions

We have presented new 3-D spherical free-subduction models with a composite viscoplastic plate and viscously layered mantle. We examined the sensitivity of subduction dynamics and trench evolution to plate age (simulated with covarying plate densities and thicknesses) and plate width.

Our results complement previous studies on the effect of age and width on the evolution of subduction zones. As plate age increases, plate strength increases and, as a result, the subduction style transitions from vertically sinking and folding to retreating with a shallower upper mantle dip angle. Our models show a tendency to produce 'C' shaped trenches for narrower plates and 'W' shaped trenches for wider plates, consistent with the models of Schellart et al. (2007). However, we also find that the effect of width is modulated by the age of the subducting plate. For young plates that are in the vertical folding regime, the trench does not develop a 'W' shape, regardless of width. 'C' or 'W'-shaped trenches are only generated in cases where the slab is able to drive trench retreat. For those cases that do retreat, younger and weaker plates develop enhanced along-strike variability in trench shape.

We now have the means to simulate subduction dynamics in a spherical shell geometry, which is appropriate for Earth's mantle. This opens up new possibilities and will

be used in the future to investigate additional factors that affect subduction dynamics and their expression at Earth's surface.

Acknowledgments

F.C. is funded by an Australian Government Research Training Program (RTP) Scholarship. D.R.D. acknowledges support from the Australian Research Council (ARC), under DP170100058. L.S. was funded by an EPSRC DTP studentship (EP/N509486/1), S.G. received support under NERC grant NE/K010743/1. Numerical simulations were undertaken on the NCI National Facility in Canberra, Australia, which is supported by the Australian Commonwealth Government. The Fluidity computational modelling framework, including source code and documentation, is available from `https://fluidityproject.github.io/`; the version used for the simulations presented herein has been archived at https://zenodo.org/record/5636819#.YYBeydZBxR4. Authors would like to thank Cian Wilson, Chris Matthews, Thomas Duvernay, Siavash Ghelichkhan, Angus Gibson and Marthe Klöcking for fruitful discussions at various stages of this research.

References

Agrusta, R., Goes, S., & van Hunen, J. (2017). Subducting-slab transition-zone interaction: Stagnation, penetration and mode switches. *Earth and Planetary Science Letters*, *464*, 10–23.

Alsaif, M., Garel, F., Gueydan, F., & Davies, D. R. (2020). Upper plate deformation and trench retreat modulated by subduction-driven shallow asthenospheric flows. *Earth and Planetary Science Letters*, *532*, 116013.

Atwater, T. (1970). Implications of plate tectonics for the Cenozoic tectonic evolution of western North America. *Geological Society of America Bulletin*, *81*(12), 3513–3536.

Balay, S., Abhyankar, S., Adams, M. F., Brown, J., Brune, P., Buschelman, K., ... Zhang, H. (2021a). *PETSc users manual* (Tech. Rep. No. ANL-95/11 - Revision 3.15). Argonne National Laboratory. Retrieved from `https://www.mcs.anl.gov/petsc`

Balay, S., Abhyankar, S., Adams, M. F., Brown, J., Brune, P., Buschelman, K., ... Zhang, H. (2021b). *PETSc Web page.* `https://www.mcs.anl.gov/petsc`. Retrieved from `https://www.mcs.anl.gov/petsc`

Balay, S., Gropp, W. D., McInnes, L. C., & Smith, B. F. (1997). Efficient management of parallelism in object-oriented numerical software libraries. In *Modern software tools for scientific computing* (pp. 163–202). Birkhauser Boston Inc.

Bayly, B. (1982). Geometry of subducted plates and island arcs viewed as a buckling problem. *Geology*, *10*(12), 629–632.

Beall, A., Fagereng, Å., Davies, J. H., Garel, F., & Davies, D. R. (2021). Influence of subduction zone dynamics on interface shear stress and potential relationship with seismogenic behavior. *Geochemistry, Geophysics, Geosystems*, *22*(2), e2020GC009267.

Becker, T. W., & Faccenna, C. (2011). Mantle conveyor beneath the tethyan collisional belt. *Earth and Planetary Science Letters*, *310*(3-4), 453–461.

Bellahsen, N., Faccenna, C., & Funiciello, F. (2005). Dynamics of subduction and plate motion in laboratory experiments: Insights into the "plate tectonics" behavior of the Earth. *Journal of Geophysical Research: Solid Earth*, *110*(B1).

Bird, P. (2003). An updated digital model of plate boundaries. *Geochemistry, Geophysics, Geosystems*, *4*(3).

Butterworth, N. P., Quevedo, L., Morra, G., & Müller, R. (2012). Influence of overriding plate geometry and rheology on subduction. *Geochemistry, Geophysics, Geosystems*, *13*(6).

Butterworth, N. P., Talsma, A. S., Müller, R. D., Seton, M., Bunge, H.-P., Schu-

berth, B. S. A., ... Heine, C. (2014). Geological, tomographic, kinematic and geodynamic constraints on the dynamics of sinking slabs. *Journal of Geodynamics*, *73*, 1–13.

Capitanio, F. A., Faccenna, C., Zlotnik, S., & Stegman, D. R. (2011). Subduction dynamics and the origin of Andean orogeny and the Bolivian orocline. *Nature*, *480*(7375), 83–86.

Capitanio, F. A., & Morra, G. (2012). The bending mechanics in a dynamic subduction system: Constraints from numerical modelling and global compilation analysis. *Tectonophysics*, *522*, 224–234.

Capitanio, F. A., Morra, G., & Goes, S. (2007). Dynamic models of downgoing plate-buoyancy driven subduction: Subduction motions and energy dissipation. *Earth and Planetary Science Letters*, *262*(1-2), 284–297.

Capitanio, F. A., Stegman, D. R., Moresi, L. N., & Sharples, W. (2010). Upper plate controls on deep subduction, trench migrations and deformations at convergent margins. *Tectonophysics*, *483*(1-2), 80–92.

Chamolly, A., & Ribe, N. M. (2021). Fluid mechanics of free subduction on a sphere. part 1. the axisymmetric case. *Journal of Fluid Mechanics*, *929*.

Čížková, H., & Bina, C. R. (2013). Effects of mantle and subduction-interface rheologies on slab stagnation and trench rollback. *Earth and Planetary Science Letters*, *379*, 95–103.

Čížková, H., & Bina, C. R. (2015). Geodynamics of trench advance: Insights from a philippine-sea-style geometry. *Earth and Planetary Science Letters*, *430*, 408–415.

Čížková, H., & Bina, C. R. (2019). Linked influences on slab stagnation: Interplay between lower mantle viscosity structure, phase transitions, and plate coupling. *Earth and Planetary Science Letters*, *509*, 88–99.

Čížková, H., van Hunen, J., & van den Berg, A. (2007). Stress distribution within subducting slabs and their deformation in the transition zone. *Physics of the Earth and Planetary Interiors*, *161*(3-4), 202–214.

Čížková, H., van Hunen, J., van den Berg, A. P., & Vlaar, N. J. (2002). The influence of rheological weakening and yield stress on the interaction of slabs with the 670 km discontinuity. *Earth and Planetary Science Letters*, *199*(3-4), 447–457.

Conrad, C. P., & Hager, B. H. (1999). Effects of plate bending and fault strength at subduction zones on plate dynamics. *Journal of Geophysical Research: Solid Earth*, *104*(B8), 17551–17571.

Cross, T. A., & Pilger, R. H. (1982). Controls of subduction geometry, location of magmatic arcs, and tectonics of arc and back-arc regions. *Geological Society of America Bulletin*, *93*(6), 545–562.

Davies, D. R., Le Voci, G., Goes, S., Kramer, S. C., & Wilson, C. R. (2016). The mantle wedge's transient 3-D flow regime and thermal structure. *Geochem. Geophys. Geosys.*, *17*, 78-100. doi: 10.1002/2015GC006125

Davies, D. R., Wilson, C. R., & Kramer, S. C. (2011). Fluidity: A fully unstructured anisotropic adaptive mesh computational modeling framework for geodynamics. *Geochemistry, Geophysics, Geosystems*, *12*(6).

Di Giuseppe, E., van Hunen, J., Funiciello, F., Faccenna, C., & Giardini, D. (2008). Slab stiffness control of trench motion: Insights from numerical models. *Geochemistry, Geophysics, Geosystems*, *9*(2).

Espurt, N., Funiciello, F., Martinod, J., Guillaume, B., Regard, V., Faccenna, C., & Brusset, S. (2008). Flat subduction dynamics and deformation of the South American plate: Insights from analog modeling. *Tectonics*, *27*(3).

Faccenna, C., Becker, T. W., Lucente, F. P., Jolivet, L., & Rossetti, F. (2001). History of subduction and back arc extension in the Central Mediterranean. *Geophysical Journal International*, *145*(3), 809–820.

Forsyth, D., & Uyeda, S. (1975). On the relative importance of the driving forces of

plate motion. *Geophysical Journal International*, *43*(1), 163–200.
Frank, F. (1968). Curvature of island arcs. *Nature*, *220*(5165), 363–363.
Fukao, Y., & Obayashi, M. (2013a). Subducted slabs stagnant above, penetrating through and trapped below the 660 km discontinuity. *J. Geophys. Res.*, *118*, 5920–5938. doi: 10.1002/2013JB010466
Fukao, Y., & Obayashi, M. (2013b). Subducted slabs stagnant above, penetrating through, and trapped below the 660 km discontinuity. *Journal of Geophysical Research: Solid Earth*, *118*(11), 5920–5938.
Fukao, Y., Obayashi, M., Nakakuki, T., & Group, D. S. P. (2009). Stagnant slab: a review. *Annual Review of Earth and Planetary Sciences*, *37*, 19–46.
Fukao, Y., Yamaoka, K., & Sakurai, T. (1987). Spherical shell tectonics: buckling of subducting lithosphere. *Physics of the earth and planetary interiors*, *45*(1), 59–67.
Funiciello, F., Faccenna, C., Heuret, A., Lallemand, S., Di Giuseppe, E., & Becker, T. W. (2008). Trench migration, net rotation and slab–mantle coupling. *Earth and Planetary Science Letters*, *271*(1-4), 233–240.
Funiciello, F., Moroni, M., Piromallo, C., Faccenna, C., Cenedese, A., & Bui, H. A. (2006). Mapping mantle flow during retreating subduction: Laboratory models analyzed by feature tracking. *Journal of Geophysical Research: Solid Earth*, *111*(B3).
Garel, F., Goes, S., Davies, D. R., Davies, J. H., Kramer, S. C., & Wilson, C. R. (2014). Interaction of subducted slabs with the mantle transition-zone: A regime diagram from 2-D thermo-mechanical models with a mobile trench and an overriding plate. *Geochemistry, Geophysics, Geosystems*, *15*(5), 1739–1765.
Garel, F., Thoraval, C., Tommasi, A., Demouchy, S., & Davies, D. R. (2020). Using thermo-mechanical models of subduction to constrain effective mantle viscosity. *Earth and Planetary Science Letters*, *539*, 116243.
Goes, S., Agrusta, R., van Hunen, J., & Garel, F. (2017). Subduction-transition zone interaction: A review. *Geosphere*, *13*(3), 644–664.
Goes, S., Capitanio, F. A., & Morra, G. (2008). Evidence of lower-mantle slab penetration phases in plate motions. *Nature*, *451*(7181), 981–984.
Goes, S., Capitanio, F. A., Morra, G., Seton, M., & Giardini, D. (2011). Signatures of downgoing plate-buoyancy driven subduction in Cenozoic plate motions. *Physics of the Earth and Planetary Interiors*, *184*(1-2), 1–13.
Gutscher, M. A., Malavieille, J., Lallemand, S., & Collot, J. Y. (1999). Tectonic segmentation of the North Andean margin: Impact of the Carnegie Ridge collision. *Earth and Planetary Science Letters*, *168*(3-4), 255–270.
Gutscher, M. A., Olivet, J. L., Aslanian, D., Eissen, J. P., & Maury, R. (1999). The "lost Inca Plateau": Cause of flat subduction beneath Peru? *Earth and Planetary Science Letters*, *171*(3), 335–341.
Hager, B. H., & Richards, A. M. (1989). Long–wavelength variations in Earth's geoid: Physical models and dynamical implications. *Phil. Trans. Roy. Soc. London, Ser. A.*, *328*, 309–327.
Heuret, A., Funiciello, F., Faccenna, C., & Lallemand, S. (2007). Plate kinematics, slab shape and back-arc stress: A comparison between laboratory models and current subduction zones. *Earth and Planetary Science Letters*, *256*(3-4), 473–483.
Heuret, A., Lallemand, S., Funiciello, F., Piromallo, C., & Faccenna, C. (2011). Physical characteristics of subduction interface type seismogenic zones revisited. *Geochemistry, Geophysics, Geosystems*, *12*(1).
Holt, A. F., & Royden, L. H. (2020). Subduction dynamics and mantle pressure: 2. towards a global understanding of slab dip and upper mantle circulation. *Geochemistry, Geophysics, Geosystems*, *21*(7), e2019GC008771.
Holt, A. F., Royden, L. H., & Becker, T. W. (2017). The dynamics of double slab subduction. *Geophysical Journal International*, *209*(1), 250–265.

Holt, A. F., Royden, L. H., Becker, T. W., & Faccenna, C. (2018). Slab interactions in 3-d subduction settings: The philippine sea plate region. *Earth and Planetary Science Letters*, *489*, 72–83.

Jarrard, R. D. (1986). Relations among subduction parameters. *Reviews of Geophysics*, *24*(2), 217–284.

Karato, S.-i., Riedel, M. R., & Yuen, D. A. (2001). Rheological structure and deformation of subducted slabs in the mantle transition zone: Implications for mantle circulation and deep earthquakes. *Physics of the Earth and Planetary Interiors*, *127*(1-4), 83–108.

Kearey, P., Klepeis, K. A., & Vine, F. J. (2009). *Global tectonics*. John Wiley & Sons.

Kimura, G., Kitamura, Y., Yamaguchi, A., Kameda, J., Hashimoto, Y., & Hamahashi, M. (2019). Origin of the early cenozoic belt boundary thrust and izanagi–pacific ridge subduction in the western pacific margin. *Island Arc*, *28*(5), e12320.

Kramer, S. C., Davies, D. R., & Wilson, C. R. (2021). Analytical solutions for mantle flow in cylindrical and spherical shells. *Geoscientific Model Development*, *14*(4), 1899–1919.

Kramer, S. C., Wilson, C. R., & Davies, D. R. (2012). An implicit free surface algorithm for geodynamical simulations. *Physics of the Earth and Planetary Interiors*, *194*, 25–37.

Lallemand, S., Heuret, A., & Boutelier, D. (2005). On the relationships between slab dip, back-arc stress, upper plate absolute motion, and crustal nature in subduction zones. *Geochemistry, Geophysics, Geosystems*, *6*(9).

Laravie, J. A. (1975). Geometry and lateral strain of subducted plates in island arcs. *Geology*, *3*(9), 484–486.

Le Voci, G., Davies, D. R., Goes, S., Kramer, S. C., & Wilson, C. R. (2014). A systematic 2-D investigation into the mantle wedge's transient flow regime and thermal structure: complexities arising from a hydrated rheology and thermal buoyancy. *Geochem. Geophys. Geosys.*, *15*, 28–51. doi: 10.1002/2013GC005022

Li, C., van der Hilst, R. D., Engdahl, E. R., & Burdick, S. (2008). A new global model for P wave speed variations in Earth's mantle. *Geochemistry, Geophysics, Geosystems*, *9*(5).

Lithgow-Bertelloni, C., & Richards, M. A. (1998). The dynamics of Cenozoic and Mesozoic plate motions. *Reviews of Geophysics*, *36*(1), 27–78.

Lonsdale, P. (2005). Creation of the Cocos and Nazca plates by fission of the Farallon plate. *Tectonophysics*, *404*(3-4), 237–264.

Mahadevan, L., Bendick, R., & Liang, H. (2010). Why subduction zones are curved. *Tectonics*, *29*(6).

Mann, P., & Taira, A. (2004). Global tectonic significance of the Solomon Islands and Ontong Java Plateau convergent zone. *Tectonophysics*, *389*(3-4), 137–190.

Martinod, J., Funiciello, F., Faccenna, C., Labanieh, S., & Regard, V. (2005). Dynamical effects of subducting ridges: insights from 3-D laboratory models. *Geophysical Journal International*, *163*(3), 1137–1150.

Martinod, J., Husson, L., Roperch, P., Guillaume, B., & Espurt, N. (2010). Horizontal subduction zones, convergence velocity and the building of the andes. *Earth and Planetary Science Letters*, *299*(3-4), 299–309.

Mason, W. G., Moresi, L., Betts, P. G., & Miller, M. S. (2010). Three-dimensional numerical models of the influence of a buoyant oceanic plateau on subduction zones. *Tectonophysics*, *483*(1-2), 71–79.

McKenzie, D., Jackson, J., & Priestley, K. (2005). Thermal structure of oceanic and continental lithosphere. *Earth and Planetary Science Letters*, *233*(3-4), 337–349.

Mitrovica, J. X., Beaumont, C., & Jarvis, G. T. (1989). Tilting of continental inte-

riors by the dynamical effects of subduction. *Tectonics*, *8*, 1079-1094. doi: 10.1029/TC008i005p01079

Morra, G., Chatelain, P., Tackley, P., & Koumoutsakos, P. (2009). Earth curvature effects on subduction morphology: Modeling subduction in a spherical setting. *Acta Geotechnica*, *4*(2), 95–105.

Morra, G., Quevedo, L., & Müller, R. D. (2012). Spherical dynamic models of top-down tectonics. *Geochemistry, Geophysics, Geosystems*, *13*(3).

Morra, G., Regenauer-Lieb, K., & Giardini, D. (2006). Curvature of oceanic arcs. *Geology*, *34*(10), 877–880.

Müller, R. D., Seton, M., Zahirovic, S., Williams, S. E., Matthews, K. J., Wright, N. M., ... Cannon, J. (2016). Ocean basin evolution and global-scale plate reorganization events since Pangea breakup. *Annual Review of Earth and Planetary Sciences*, *44*, 107–138.

Müller, R. D., Zahirovic, S., Williams, S. E., Cannon, J., Seton, M., Bower, D. J., ... Gurnis, M. (2019). A global plate model including lithospheric deformation along major rifts and orogens since the Triassic. *Tectonics*, *38*(6), 1884–1907.

Neal, C. R., Mahoney, J. J., Kroenke, L. W., Duncan, R. A., & Petterson, M. G. (1997). The Ontong Java Plateau. *Geophysical Monograph-American Geophysical Union*, *100*, 183–216.

OzBench, M., Regenauer-Lieb, K., Stegman, D. R., Morra, G., Farrington, R., Hale, A., ... Moresi, L. (2008). A model comparison study of large-scale mantle–lithosphere dynamics driven by subduction. *Physics of the Earth and Planetary Interiors*, *171*(1-4), 224–234.

Pelletier, B., Calmant, S., & Pillet, R. (1998). Current tectonics of the Tonga–New Hebrides region. *Earth and Planetary Science Letters*, *164*(1-2), 263–276.

Perrin, A., Goes, S., Prytulak, J., Rondenay, S., & Davies, D. R. (2018). Mantle wedge temperatures and their potential relation to volcanic arc location. *Earth and Planetary Science Letters*, *501*, 67–77.

Ribe, N. M. (2010). Bending mechanics and mode selection in free subduction: A thin-sheet analysis. *Geophysical Journal International*, *180*(2), 559–576.

Rodríguez-González, J., Negredo, A. M., & Billen, M. I. (2012). The role of the overriding plate thermal state on slab dip variability and on the occurrence of flat subduction. *Geochemistry, Geophysics, Geosystems*, *13*(1).

Rubey, M., Brune, S., Heine, C., Davies, D. R., Williams, S. E., & Müller, R. D. (2017). Global patterns in Earth's dynamic topography since the Jurassic: the role of subducted slabs. *Solid Earth*, *8*, 899-919. doi: 10.5194/se-8-899-2017

Schellart, W. P. (2004). Kinematics of subduction and subduction-induced flow in the upper mantle. *Journal of Geophysical Research: Solid Earth*, *109*(B7).

Schellart, W. P. (2008). Kinematics and flow patterns in deep mantle and upper mantle subduction models: Influence of the mantle depth and slab to mantle viscosity ratio. *Geochemistry, Geophysics, Geosystems*, *9*(3).

Schellart, W. P., Freeman, J., Stegman, D. R., Moresi, L., & May, D. (2007). Evolution and diversity of subduction zones controlled by slab width. *Nature*, *446*(7133), 308–311.

Schepers, G., van Hinsbergen, D. J., Spakman, W., Kosters, M. E., Boschman, L. M., & McQuarrie, N. (2017). South-American plate advance and forced Andean trench retreat as drivers for transient flat subduction episodes. *Nature communications*, *8*(1), 1–9.

Schettino, A., & Tassi, L. (2012). Trench curvature and deformation of the subducting lithosphere. *Geophysical Journal International*, *188*(1), 18–34.

Scholl, D. W., Buffington, E. C., & Marlow, M. S. (1975). Plate tectonics and the structural evolution of the Aleutian–Bering Sea region. *Geological Society of America Special Papers*, *151*, 1–32.

Sdrolias, M., & Müller, R. D. (2006). Controls on back-arc basin formation. *Geochemistry, Geophysics, Geosystems*, *7*(4).

Sharples, W., Jadamec, M. A., Moresi, L.-N., & Capitanio, F. A. (2014). Overriding plate controls on subduction evolution. *Journal of Geophysical Research: Solid Earth*, *119*(8), 6684–6704.

Stegman, D. R., Farrington, R., Capitanio, F. A., & Schellart, W. P. (2010). A regime diagram for subduction styles from 3-D numerical models of free subduction. *Tectonophysics*, *483*(1-2), 29–45.

Stegman, D. R., Freeman, J., Schellart, W. P., Moresi, L., & May, D. (2006). Influence of trench width on subduction hinge retreat rates in 3-D models of slab rollback. *Geochemistry, Geophysics, Geosystems*, *7*(3).

Stegman, D. R., Schellart, W. P., & Freeman, J. (2010). Competing influences of plate width and far-field boundary conditions on trench migration and morphology of subducted slabs in the upper mantle. *Tectonophysics*, *483*(1-2), 46–57.

Stern, R. J. (2002). Subduction zones. *Reviews of geophysics*, *40*(4), 3–1.

Stotz, I. L., Iaffaldano, G., & Davies, D. R. (2017). Late Miocene Pacific plate kinematic change explained with coupled global models of mantle and lithosphere dynamics. *Geophysical Research Letters*, *44*(14), 7177–7186.

Strak, V., & Schellart, W. P. (2016). Control of slab width on subduction-induced upper mantle flow and associated upwellings: Insights from analog models. *Journal of Geophysical Research: Solid Earth*, *121*(6), 4641–4654.

Suchoy, L., Goes, S., Chen, F., & Davies, R. (2022). How aseismic ridges modify the dynamics of free subduction: a 3-d numerical investigation. *Frontiers in Earth Science*, 611.

Suchoy, L., Goes, S., Maunder, B., Garel, F., & Davies, R. (2021). Effects of basal drag on subduction dynamics from 2d numerical models. *Solid Earth*, *12*(1), 79–93.

Tanimoto, T. (1998). State of stress within a bending spherical shell and its implications for subducting lithosphere. *Geophysical Journal International*, *134*(1), 199–206.

Torii, Y., & Yoshioka, S. (2007). Physical conditions producing slab stagnation: Constraints of the Clapeyron slope, mantle viscosity, trench retreat, and dip angles. *Tectonophysics*, *445*(3-4), 200–209.

Tosi, N., Stein, C., Noack, L., Hüttig, C., Maierová, P., Samuel, H., ... Tackley, P. J. (2015). A community benchmark for viscoplastic thermal convection in a 2-d square box. *Geochemistry, Geophysics, Geosystems*, *16*(7), 2175-2196. doi: 10.1002/2015GC005807

van der Hilst, R., & Seno, T. (1993). Effects of relative plate motion on the deep structure and penetration depth of slabs below the Izu-Bonin and Mariana island arcs. *Earth and Planetary Science Letters*, *120*(3-4), 395–407.

van der Meer, D. G., van Hinsbergen, D. J., & Spakman, W. (2018). Atlas of the underworld: Slab remnants in the mantle, their sinking history, and a new outlook on lower mantle viscosity. *Tectonophysics*, *723*, 309–448.

van Dinther, Y., Morra, G., Funiciello, F., & Faccenna, C. (2010). Role of the overriding plate in the subduction process: Insights from numerical models. *Tectonophysics*, *484*(1-4), 74–86.

van Hunen, J., van den Berg, A. P., & Vlaar, N. J. (2002). On the role of subducting oceanic plateaus in the development of shallow flat subduction. *Tectonophysics*, *352*(3-4), 317–333.

Wheeler, P., & White, N. (2002). Measuring dynamic topography: An analysis of Southeast Asia. *Tectonics*, *21*(5), 4–1.

Whittaker, J. M., Müller, R. D., Sdrolias, M., & Heine, C. (2007). Sunda-Java trench kinematics, slab window formation and overriding plate deformation since the Cretaceous. *Earth and Planetary Science Letters*, *255*(3-4), 445–457.

Wilson, C. R. (2009). *Modelling multiple-material flows on adaptive unstructured meshes*. PhD Thesis, Imperial College London, UK.

Yamaoka, K. (1988). Spherical shell tectonics: on the buckling of the lithosphere at subduction zones. *Tectonophysics*, *147*(3-4), 179–191.